Tectonophysics 722 (2018) 210–226

Contents lists available at ScienceDirect

Tectonophysics

journal homepage: www.elsevier.com/locate/tecto

Variable slip-rate and slip-per-event on a plate boundary fault: The Dead Sea fault in northern Israel

Neta Wechsler[a,*], Thomas K. Rockwell[b], Yann Klinger[c]

[a] Tel-Aviv University, Department of Geosciences, Tel-Aviv 69978, Israel
[b] San Diego State University, 5500 Campanile Dr., San Diego, CA 92182, USA
[c] Institut de Physique du Globe de Paris, 1 rue Jussieu, Paris 75005, France

ARTICLE INFO

Keywords:
Palaeoseismology
Earthquake interaction and forecasting
Transform faults
Geomorphology

ABSTRACT

We resolved displacement on buried stream channels that record the past 3400 years of slip history for the Jordan Gorge (JGF) section of the Dead Sea fault in Israel. Based on three-dimensional (3D) trenching, slip in the past millennium amounts to only 2.7 m, similar to that determined in previous studies, whereas the previous millennium experienced two to three times this amount of displacement with nearly 8 m of cumulative slip, indicating substantial short term variations in slip rate. The slip rate averaged over the past 3400 years, as determined from 3D trenching, is 4.1 mm/yr, which agrees well with geodetic estimates of strain accumulation, as well as with longer-term geologic slip rate estimates. Our results indicate that: 1) the past 1200 years appear to significantly lack slip, which may portend a significant increase in future seismic activity; 2) short-term slip rates for the past two millennia have varied by more than a factor of two and suggest that past behavior is best characterized by clustering of earthquakes. From these observations, the earthquake behavior of the Jordan Gorge fault best fits is a "weak segment model" where the relatively short fault section (20 km), bounded by releasing steps, fails on its own in moderate earthquakes, or ruptures with adjacent segments.

1. Introduction

Understanding the irregular occurrence of large and damaging earthquakes in space and time on plate boundary faults is a long-standing critical problem in earthquake research. Simple elastic loading models predict fairly regular recurrence of slip events (Reid, 1910; Ben-Zion and Rice, 1993), but most long earthquake records exhibit substantial variability in the timing of past surface ruptures (Fumal et al., 2002; Rockwell et al., 2015; Scharer et al., 2007; Sieh, 1984), although displacement per event appears to be more repeatable (Hecker et al., 2013; Klinger et al., 2011; Salisbury et al., 2012). One problem is that most long paleoseismic records have been developed on only a few faults, so additional examples are required to better understand the variability of earthquake recurrence in time and space.

The Dead Sea Transform fault (DST) in northern Israel (Fig. 1) is an ideal plate boundary structure to study long-term fault behavior and earthquake sequences because: 1) there is a long (> 2000 year) record of historical earthquakes for the whole region; 2) there are additional earthquake records from seismites that offer a very precise record of strong shaking at various locations around the Dead Sea (Agnon, 2014; Kagan et al., 2011); and 3) there is a growing body of archaeoseismic and paleoseismic data that document both timing and displacement for some sections of the fault zone (Daëron et al., 2005; Daëron et al., 2007; Elias et al., 2007; Ellenblum et al., 2015; Ferry et al., 2007; Ferry et al., 2011; Gomez et al., 2007; Klinger et al., 2015; Marco et al., 2005; Nemer et al., 2008; Nemer and Meghraoui, 2006; Wechsler et al., 2014; Wechsler and Marco, 2017; Zilberman et al., 2000). The DST is capable of generating magnitudes larger than M7, such as the 1995 Aqaba earthquake (Hofstetter, 2003), and is known to have caused significant structural damage and loss of life in the past (Ambraseys, 2009, Amiran et al., 1994, Guidoboni, 1994). Furthermore, the slip rate on the DST is about 4–5 mm/yr, which means that large earthquakes will occur less frequently and can be adequately resolved with modern ^{14}C dating methods and tied to known historical earthquakes, in contrast to fast moving faults where the probability distributions of the event ages commonly overlap.

The Jordan Gorge fault (JGF) is a relatively unique structure along the DST, as the plate boundary is fairly simple to the south in the Jordan and Arava Valleys, but is complex and multi-stranded to the north in Lebanon (Fig. 1b). Furthermore, the 20 km-long JGF is bounded both to the north and south by releasing steps in Hula Basin and the Sea of Galilee, respectively. Additionally, the northernmost part

* Corresponding author.
E-mail address: netawe@post.tau.ac.il (N. Wechsler).

https://doi.org/10.1016/j.tecto.2017.10.017
Received 30 November 2016; Received in revised form 15 September 2017; Accepted 19 October 2017
Available online 27 October 2017
0040-1951/

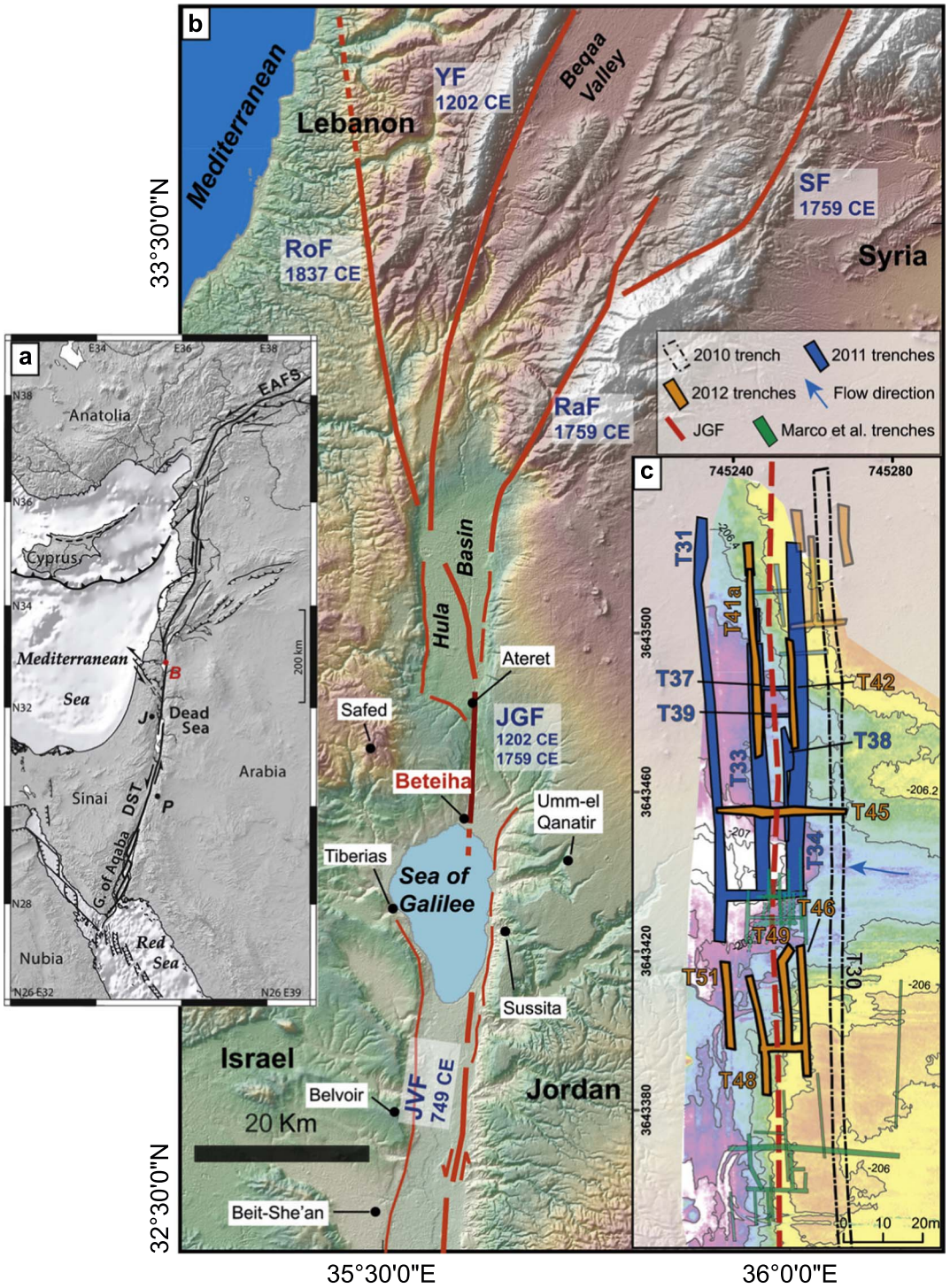

Fig. 1. a) Plate tectonic settings of the Middle East, with major faults. EAFS – East Anatolia Fault; DST – Dead Sea Transform; J – Jerusalem. K – Kerak; P – Petra. B – Beteiha trench site. b) Location of major and minor faults of the DST in the vicinity of Hula basin and the Sea of Galilee. JGF, Jordan Gorge fault; JVF, Jordan Valley fault; RaF, Rachaya fault; RoF, Roum fault; SF, Serghaya fault; YF, Yammouneh fault. The latest earthquake known to have ruptured is mentioned below each fault name. Topography from ASTER GDEM (ASTER GDEM is a product of Ministry of Economy, Trade, and Industry [METI] and National Aeronautics and Space Administration [NASA]). c) Map of the Beteiha paleoseismic site with outlines of all trenches dug during the 3-year campaign, and the approximate location (based on air photos) of the trenches of Marco et al. (2005). The trenches discussed in this paper are highlighted and labeled. Topography model was obtained using TLS (Terrestrial Laser Scanner) prior to 2nd year trenching, courtesy of O. Katz from the Geological Survey of Israel. The contour lines represent elevation b.m.s.l.

of the Jordan Valley fault (JVF) section of the DST, immediately south of the Sea of Galilee, is creeping at about 2 mm/yr (Hamiel et al., 2016). Thus, the JGF section of the DST may be expected to fail on its own in moderate earthquakes, as in 1759 (Ellenblum et al., 1998), or in conjunction with fault ruptures from the north (the common era (CE) 1202 earthquake; Ellenblum et al., 1998, Daëron et al., 2005) or south (the 749 CE and 363 CE earthquakes; Wechsler and Marco, 2017).

In this paper, we present new observations on timing and displacement on the JGF section of the DST in Beteiha Valley on the north shore of the Sea of Galilee. We have systematically excavated several fluvial channels that crossed the fault at a high angle on the flood plain of the Jordan River to resolve displacement across the fault for each

Table 1
The channels found at the Beteiha site, with ages and general descriptions. (Modified from Wechsler et al., 2014).

Channel	Age	General description	Comments
CH1	9th–14th century CE	A gravelly sandy channel complex, many freshwater molluscs shells	Previously studied channels by Marco et al. (2005), captures the 1202 and 1759 CE earthquakes
CH2	7th–8th century CE	A sandy channel	Cuts the northern margin of CH3, east of the fault.
CH3	5th–7th century CE	A gravelly sandy channel complex with cross-cutting units	South margin cut by CH1, north margin by CH2. Channel stratigraphy record evidence for 2 earthquake ruptures.
CH4	1st–4th century CE	A sandy gravelly channel complex	Better preserved west of the fault due to vertical offset. Channel stratigraphy record evidence for 6 earthquake ruptures. Slip resolved for two of them.
CH5	1st–3rd century CE	A V-shaped gravelly channel, possibly man-made	Only trenched east of the fault, not discussed in this paper.
CH6	10th–4th century BCE	Distinct red unit, more of a flood surface than a channel	Divided into 2 sub units, which are at different depths. Used to constrain CH4 age as it appears directly below it.
CH7	3500–5300 years BP	A sandy channel, very wide	South of CH1–4, distinct. Resolves a medium term slip rate.

channel. The channels represent a record of nearly continuous fluvial flow for the past 2000 years, and their ages are presented in Table 1, compiled from Wechsler et al. (2014) and Marco et al. (2005). We have also resolved displacement on a ~3400 year-old channel that yields a longer-term slip rate that closely matches the geodetic rate for the fault in this region. From these new data, we evaluate the short and long term behavior of the JGF and compare to the results of other studies worldwide.

2. Geological settings

The Dead Sea Transform is the plate boundary fault between the Arabian and African plates (Quennell, 1956; Fig. 1a). Average strain accumulation, at about 4–6 mm/yr, appears to be consistent at different time scales, from decadal measurements (Le Beon et al., 2008; McClusky et al., 2003; Reilinger et al., 2006) to geological time scales (Le Beon et al., 2010, Le Beon et al., 2012). Motion on the DST is believed to have begun in early Miocene time, accruing about 105 km of total slip (Freund et al., 1968; Garfunkel, 1981; Garfunkel et al., 1981). Although seismically active and the source of several large and destructive earthquakes in the historical period (Ambraseys, 2009; Amiran et al., 1994; Guidoboni, 1994), the largest onshore instrumentally recorded earthquake is the 1927 M6.1 Jericho earthquake, for which no indication of surface deformation was found (Shapira et al., 1993).

The JVF section extends from the Dead Sea pull-apart basin to the Sea of Galilee and is a relatively straight and simple section of the DST (Fig. 1b). The northern-most part of the JVF appears to experience surficial creep at about 2 mm/yr in the top 2 km, with elastic loading accounting for the rest of the 4–6 mm/yr slip rate (Hamiel et al., 2016). The Sea of Galilee represents another pull-apart basin at a left step in the DST, although the 1 km width of the step is considerably smaller than that of the Dead Sea. Some historical earthquakes north of the Sea of Galilee are inferred to have not ruptured into the Jordan Valley; the 1202 CE earthquake produced over 2 m of slip where it enters the Sea from the north (Marco et al., 2005) but there is no evidence that it propagated south of the Sea of Galilee, as there is a lack of damage to the contemporaneous crusader castle of Belvoir (Fig. 1b), situated only 13 km south of the lake (Shmuel Marco, personal comm.). The combination of the releasing step and a component of creep on the Jordan Valley section immediately south of the step may account for the termination of the 1202 earthquake at the step-over, in spite of its relatively small size. As several other notable historical earthquakes appear to have been limited to the Jordan Valley (1033, 747/749 and 363 CE; Ambraseys, 2009, Amiran et al., 1994, Guidoboni, 1994), we consider the Sea of Galilee to represent a resilient segment boundary.

In Beteiha Valley, the site of our investigation, the JGF is straight and simple through Jordan Gorge to the Hula Basin, where the main fault bends or steps left to the Yammouneh fault, which continues up through the Bekka Valley. In the vicinity of Hula Basin, the DST splays into at least three major fault strands; the Roum fault on the west, the Yammouneh fault in the middle, and the Rachaya (Si'on) fault on the east. Slip is partitioned among these three strands, although the majority of strain accumulation is interpreted to continue up the Yammouneh fault (Daëron et al., 2004). North of Lebanon, the slip rate at geologic and decadal time scales seems to diverge with the latter being significantly slower (Alchalbi et al., 2010). Notably, Hamiel et al. (2016) document the absence of creep along the DST in the region of our study. From this, we infer that all slip measurements that we document on offset fluvial channels in our 3D trenching study are the result of coseismic slip events during earthquakes.

3. Paleoseismic investigations

3.1. Previous work

The work presented in this paper adds to a body of work presented in Marco et al. (2005) and Wechsler et al. (2014). Marco et al. (2005) resolved the timing and displacement for three channels that were offset in the 1202 and 1759 earthquakes, with displacements of about 2.2 and 0.5 m of left lateral movement, respectively. Wechsler et al. (2014) extended the record of the timing of past earthquakes to the previous millennium, documenting up to eight additional surface ruptures at the Beteiha site. In this paper, we use the radiocarbon data from Wechsler et al. (2014) (Table 2) along with the 3D excavations of fluvial channels to refine the earthquake history in the previous millennium, as well as to resolve displacement for most of the earthquake ruptures.

3.2. Current work

Fig. 1c summarizes the overall trench layout at the site. For detailed site description, see the “site description” section and Fig. 2a in Wechsler et al. (2014). Whereas Wechsler et al. (2014) described the evidence for earthquake history based on cross-fault stratigraphy of buried channels at the Beteiha site, here we focus on the results of our 3D trenching that follows these buried channels across the fault. Hence, the following sections describe only geometric relations between channels and channel offset measurements. Most of the dating information relies on results included in Wechsler et al. (2014) that are summarized in Tables 1 and 2. Additional dates for older channel forms that were not described by Wechsler et al. (2014) were modeled separately and will be discussed in the text.

The stratigraphy at the Beteiha paleoseismic site is characterized by massively bedded lacustrine clay deposited during high-stands of the Sea of Galilee, into which several incised channels filled with gravel and sand were later buried (Fig. 2). We mapped seven buried channels; their ages and general descriptions are summarized in Table 1 and they are numbered according to their relative age from Ch1 (youngest) to Ch7

Table 2
Results of Radiocarbon dating and OxCal modeling of samples – differences in channels 2 and 3 from Table 2 in Wechsler et al. (2014) are underlined.[a] (See Fig. S2 for the Oxcal model).

Channel	Sample number	Location	Stratigraphic unit[b]	$d^{13}C$	Age BP	Modeled calibrated age (± 2σ)[c]
2	110	T30W	260 (220)	–	1270 ± 35	673–760 (682–773) CE
	23	T30W	270–78 (250)	–	1290 ± 50	672–760 (681–774) CE
	134	T30W	270–78 (250)	− 25.9	1295 ± 20	671–762 (681–771) CE
	127	T33W	270	− 26.5	1285 ± 15	673–761 CE
	77	T34E	274	− 28.0	1285 ± 15	673–761 CE
3	99	T34W	323	–	1315 ± 20	654–694 (655–700) CE
	133	T30W	335	− 26.0	1430 ± 20	596–654 (595–652) CE
	330	T45S	340	− 23.9	1440 ± 20	589–650 (586–649) CE
	309	T45S	340	− 24.0	1465 ± 15	574–639 CE
	305	T45S	360	− 23.9	1500 ± 15	548–602 CE
	111	T33W	385	− 27.1	1555 ± 15	435–547 CE
	29	T30W	385	–	1560 ± 35	428–553 CE
	339	T45S	385	− 26.2	1570 ± 20	433–541 CE
	106	T30W	387	− 22.5	1565 ± 20	433–543 CE
	335	T45S	395	− 21.4	1545 ± 20	435–556 CE
7	521	T51W	720	–	3200 ± 20	1506–1430 BCE
	452	T46W	720	− 25.0	3520 ± 20	1904–1768 BCE
	524	*T51E*	*720*	*− 26.5*	*4095 ± 20*	–
	456	*T48W*	*720*	–	*4400 ± 60*	–
	60	T30W	749	− 23.4	3560 ± 20	1966–1830 BCE
	57	T30W	749	–	3690 ± 20	2142–1985 BCE
	463	T49E	765	− 21.8	4470 ± 15	3330–3029 BCE

[a] AMS measurements were made at the Keck carbon cycle AMS facility at UC Irvine. Ages were calibrated using OxCal 4.2.4 (Bronk-Ramsey, 2009) and calibration curve INTCAL13 (Reimer et al., 2013). Samples in italics were considered outliers and their ages were not modeled.
[b] Changes in unit designation are underlined; old unit designation in parentheses (Wechsler et al., 2014).
[c] Changes in modeled dates are underlined; old modeled dates are in parentheses (Wechsler et al., 2014).

(oldest). Collectively, offset of these channels and lake deposits record the nearly complete earthquake history for the past 2000 years, and the displacement history for the past 4000 years.

In order to reconstruct the original form of channel flow across the fault, prior to their being offset by the lateral fault movement, we used Petrel™, a software program originally used for seismic interpretation in the oil and gas industry. We first built a 3D model of the site in Petrel™ using the trench logs and DGPS coordinates from survey data presented in Wechsler et al. (2014). We then mapped the channel forms and distinct sub-channel units (when applicable) from the logs as horizons

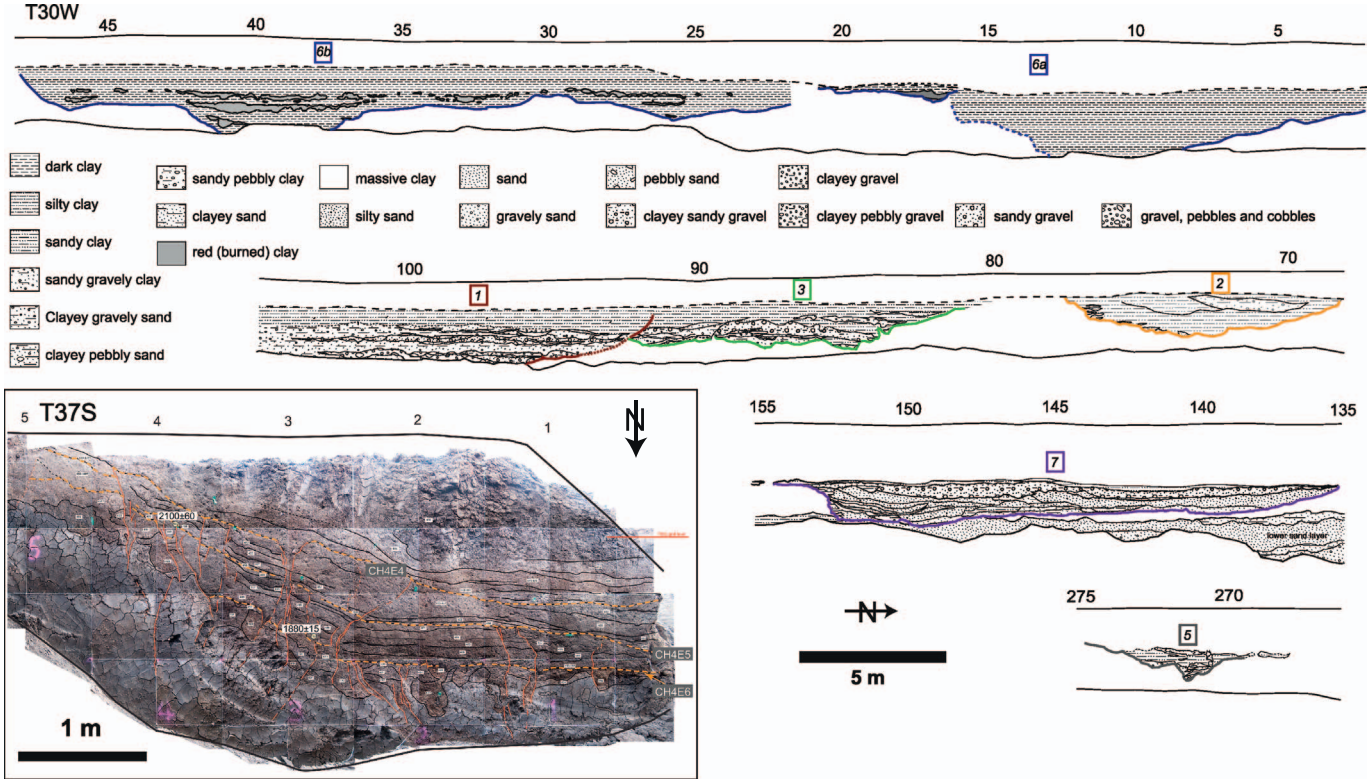

Fig. 2. A simplified log of the parts of the west wall of T30 where channels cut into the massive clay. Channels are marked by their corresponding numbers in the text. The legend is the same as in Wechsler et al. (2014). Channel 4 was not exposed in T30. Inset on lower left – an example partial photolog of T37S, where the coarse sediments of channel 4 can be seen in fault contact. Faults are marked in red, event horizons in orange (full log was published in Wechsler et al., 2014). (For interpretation of the references to color in this figure legend, the reader is referred to the web version of this article.)

and used the picked horizons to reconstruct curved surfaces that fit those horizons and represent the channel outline, by using the surface generation toolbox, constraining it to horizons extent and choosing the convergent interpolation algorithm (least squares with Briggs bi-harrmonic filter) with 0.5 m × 0.5 m grid cells. This choice of all-purpose algorithm ensures that the generated surface passes as close to the original points with less than a specified distance (in this case – 10 cm), and we did not further smooth the results. We then used those surfaces to reconstruct the horizontal movements and to measure the amount of slip for each channel form we could map. In some cases, the edges of channels or units could not be determined, either due to faulting or due to erosion by younger sediments. In that case, the thalweg form was used exclusively. Offset estimates were made by first choosing the best fit for each reconstructed feature (thalweg, channel margin or the general modeled channel shape) and using that value as the estimated best guess, with uncertainty margins (error).

3.3. Channel displacements and ages

General descriptions of the channels are summarized in Table 1. Detailed trench logs are available in the E. supp. of this paper, Fig. S1 and unit descriptions are in Table S2. In the following section, we describe the channel reconstructions along with the channel ages and their relationships to the offsets, and then follow with probable correlations to historical earthquakes.

3.3.1. Channel 1 complex

We define the Channel 1 complex as a group of channels that were previously excavated and described as CH2, CH3 and CH4 by Marco et al. (2005), the margins or portions of which were exposed in trenches T30 through T34. These channels contained pieces of detrital charcoal that yielded dates ranging from the 9th century to at least as young as the 14th century CE, when the channel complex was buried by lake deposits during an historically high period in the lake level of the Sea of Galilee. We only dated one sample from the upper part and close to the north margin of Channel 1 in trench T30, which yielded an age range of 1036–1165 CE, consistent with earlier results. For our analysis, we base our interpretations for the age of the channel complex on the dates published in Marco et al. (2005). The dates all indicate a 12–13th century CE event, which is most likely the 1202 CE earthquake based on the historical and archaeological evidence from Ateret (Ellenblum et al., 1998).

The Channel 1 units were extensively excavated in the previous trenching campaign and therefore the only usable feature for offset reconstruction in our study was the channel complex's northern margin, which cuts into the sediments of Channel 3 (examples seen in trench logs T30, T34, and T38, Figs. 2 and S1). Reconstruction of the northern margin of channel 1 by projection of the channel edge into the fault results in a horizontal offset of 2.6 ± 0.3 m (Fig. 3a, b), consistent with the 2.7 m that was previously estimated by Marco et al. (2005). We therefore are in agreement as to both the timing and the horizontal offset for the two most recent events at the site. Vertical offset could not be determined in our study due to lack of piercing points, but was apparently minor based on the Marco et al. (2005) study where the channel margins were mapped and showed about 30 cm of down-to-the-west displacement.

3.3.2. Channel 2

Channel 2 is 7–10 m wide and has a well-defined channel form. It was exposed in trenches T30, T31, T33, T34 and T38, all of them parallel to the fault. The channel fill is mostly sandy to silty in texture, with a middle layer of dark clay with a fire-oxidized burned appearance in places. The units associated with channel 2 are numbered 200–299 (Fig. S1, Table S2), with increasing numbers indicating increasing stratigraphic depth. Channel 2 cuts the north edge of channel 3 in all exposures except the easternmost one (T30). West of the fault, the gravelly-pebbly lower units of channel 3 can be seen under channel 2 (T33). Near the fault zone, the north edge of channel 2 is cut by a fault (T38W log).

Most of the dates from channel 2 infill fall within a short, 100-year time period centered around 700–720 CE, indicating that this channel represents a fairly short period of flow (for a discussion concerning inheritance in ^{14}C ages, see Wechsler et al., 2014). We did not trench within channel 2 across the fault, but from cross-cutting relations, we inferred that channel 2 is younger than channel 3, as it cuts and erodes channel 3's northern edge.

Reconstruction of the shape and thalweg of channel 2 indicates a horizontal offset of 4.0 ± 0.6 m and a vertical displacement of about 0.6 m (Fig. 3c). We interpret the ~1.3 m of additional offset over that of the channel 1 complex to represent slip from at least one additional earthquake. However, as we have no exposure of channel 2 across the fault, we cannot preclude that this offset may represent slip from two events of smaller magnitude, similar to that which occurred with the 1759 earthquake.

3.3.3. Channel 3

Channel 3 is a gravelly-sandy channel complex that was exposed in several fault-parallel trenches (T30, T33, T34 and T38) and in one fault-crossing trench (T45). The sub-units in channel 3 were numbered 300–399 for reference, with increasing numbers indicating increasing stratigraphic depth. The fault-crossing trench (T45, Figs. 3 and S1a, b in Wechsler et al., 2014) exposed the longitudinal profile of Channel 3, and faulted sediments in this exposure were used to study the earthquake history while channel 3 was an active stream (Wechsler et al., 2014). Channel 3 was divided into lower and upper units based on channel morphology, with the upper units (units 310–329) cutting into and eroding the lower units (units 330–399) east of the fault (Fig. 3 in Wechsler et al., 2014). The upper strata were not observed in fault contact on the west side of the fault. The youngest units (300–309) cap the faults on the west side and appear unrelated to the other upper channel 3 units. The strata in channel 3 vary in composition from large, rounded pebbles and cobbles at the base of individual sub-channels in the lower part of the section, to foreset-bedded gravelly sand and silty-clay in the upper part. Furthermore, the upper part of channel 3 exhibits an anomalous trend on the east side of the fault zone, with indications of a local along-fault flow direction (N to S) (Fig. 3).

There are two event horizons recorded in Channel 3 sediments, named CH3-E1 and CH3-E2 by Wechsler et al. (2014). The older event, CH3-E2, occurs within lower Channel 3 sediments, and its age is well constrained by ^{14}C ages that date the event to the sixth century CE. The younger event, CH3-E1, is capped by sandy units 300–309 and while we previously assumed that sample 99 from unit 323 represented an upper age bound for this event (Wechsler et al., 2014), a re-examination of the unit relations, and based on the measured reconstructed offset of upper channel 3 deposits, we now think that units 300–309 are in fact a much younger capping stratum, possibly even younger than Channel 2. Therefore, we conclude that unit 323 is below the event horizon of CH3-E1, and the event age is younger than previously inferred, as discussed below.

The shape of the upper units of Channel 3 forms a well-defined thalweg west of the fault, with distinctive cross-bedded sands and gravels (units 320–325). East of the fault, the channel form is not as well-defined, perhaps due to ponding and an avulsion of the channel in the fault-zone due to a slip event. The units are mapped in T30, T31, T33, T34, T38 and T45. The estimated horizontal offset is $4.0^{+0.5}/_{-1.3}$ m (Fig. 3d) and the vertical offset is about 1 m. The only ^{14}C sample that we dated from those units is the aforementioned sample 99, with an un-modeled calibrated age of 658–766 CE. This falls within the age range of Channel 2 and suggests that the upper strata in Channel 3 also cap the strata in Channel 2. The unit age along with the nearly identical horizontal offset of Channel 2 and upper Channel 3, made us re-evaluate the timing of event CH3-E1, or at least regard it as

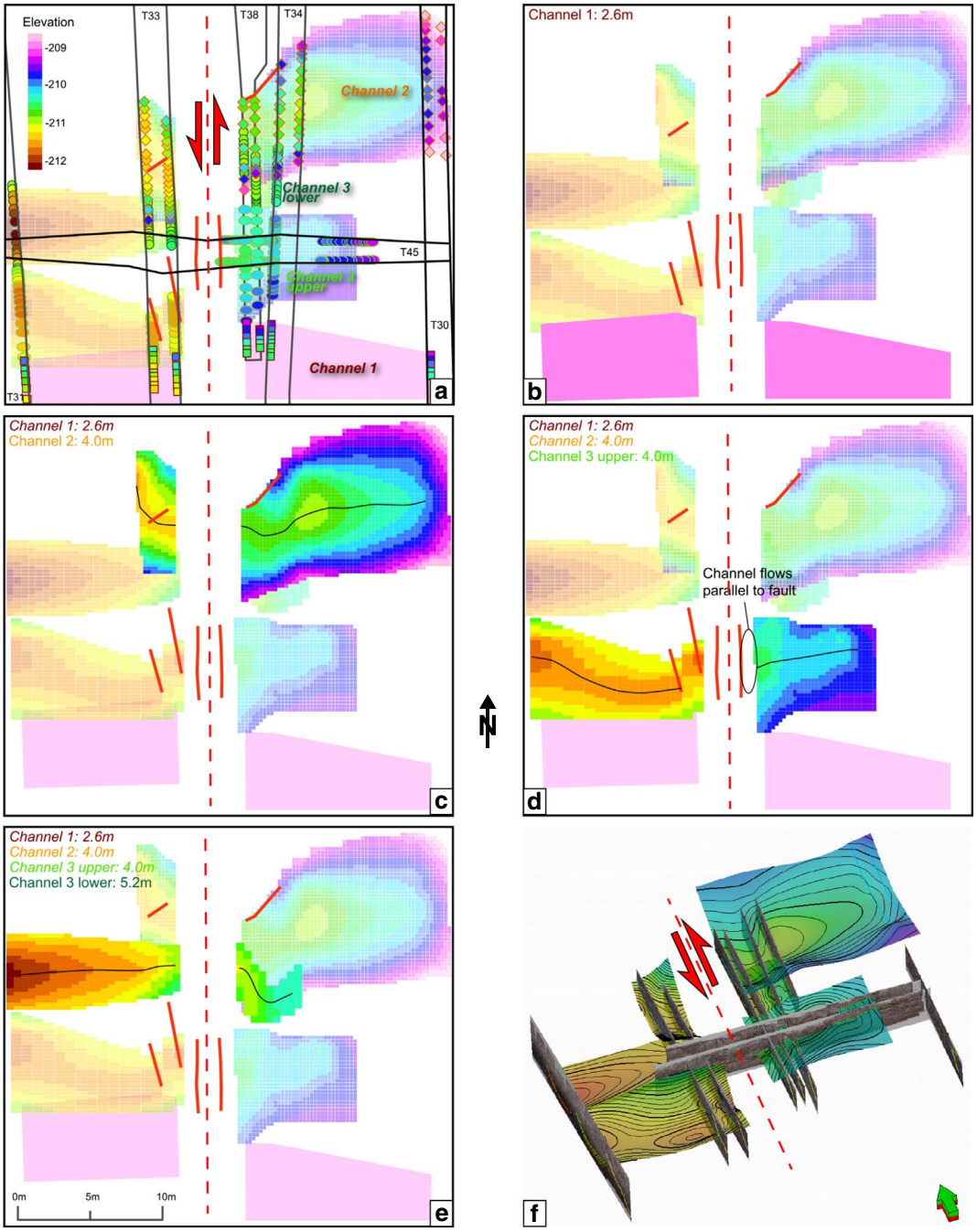

Fig. 3. Offset reconstructions for channels 1–3. Trench walls are marked by black lines, faults by red lines. In parts b–e, the features on west side are moved north incrementaly in order to rematch each two channel parts as we interpret their reconstructed shape. Horizontal offset reconstructions are written at the top left corner of each panel. Reconstructed surfaces are color-coded by elevation; scale is the same for all figures. The reconstructed feature in each panel is highlighted, and the thalweg marked by a black line, when mapped. a) Overview map of the trenches and channels. Filled circles are actual measurement points of channel shape, their fill corresponds to the elevation and their shapes represent different channels (Rectangle - Channel 1; Diamond - Channel 2; Ellipse - upper Channel 3; Cirle - lower Channel 3). b) Reconstruction of channel 1, north margin. c) Reconstruction of channel 2. d) Reconstruction of channel 3, upper units. e) Reconstruction of channel 3, lower unit. f) An example of the 3D model of trench logs and surfaces in Petrel™. (For interpretation of the references to color in this figure legend, the reader is referred to the web version of this article.)

a much smaller event with insignificant horizontal offset. The channel avulsion to the north (from Channel 3 to Channel 2) and some difference in the amount of vertical offset between the two channels may indicate an additional event. However, the avulsion could have been caused by up-stream changes and the vertical separation may be partially apparent, due to stronger channelization of upper Channel 3. Consequently we modified the OxCal model of Wechsler et al. (2014) and add event CH2-E1, which post-dates Channel 2 and pre-dates Channel 1. This event is inferred from the difference in offsets between Channels 1 and 2, without cross-fault evidence of an event horizon, unless CH3-E1 is actually the same event. This proposition cannot be resolved due to the lack of dates from the capping units 300–309. We therefore consider CH3-E1 as a marginally possible small event that is dated post-Channel 3 but pre-Channel 2. The revised OxCal model for channels 2 and 3 is presented and compared with Wechsler et al. (2014) in Table 2 and a visual comparison in Fig. 4.

The thalweg of the lower units (390–399) was mapped in T30, T31, T33, and T38. These units are characterized by mud-supported gravel

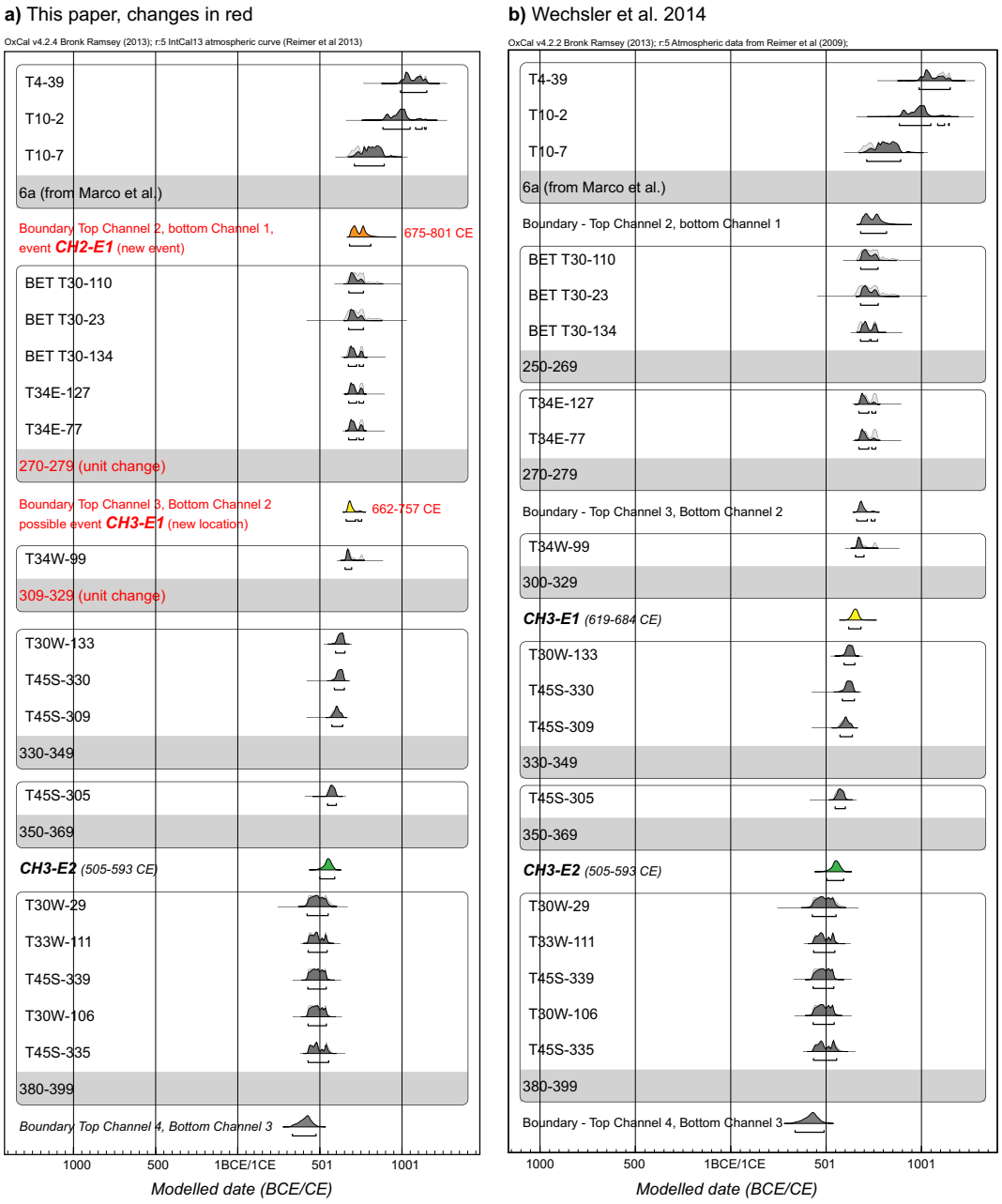

Fig. 4. A comparison between (a) the revised OxCal model for channels 2 and 3 and (b) the Wechsler et al. (2014) model version, corresponding to Table 2. Changes are marked in red. (For interpretation of the references to color in this figure legend, the reader is referred to the web version of this article.)

and rounded pebbles. Parts of the lower channel 3 deposits were eroded by Channel 2 but the channel form and thalweg could be reconstructed. The estimated horizontal offset for the thalweg gravel is $5.2^{+0.9}/_{-0.3}$ m (Fig. 3e) and the vertical offset is about 1 m. Most of the vertical displacement occurs between trenches T34 and T38, which are only a meter apart. Those trenches are east of the main fault zone, and there is evidence of secondary faulting in those trenches that explains the vertical separation across a short distance, which is also observed in trench T45. Radiocarbon dates from those units yield mid-5th to mid-6th century CE ages. Based on the dates and stratigraphic relationships, we attribute the additional offset of the lower Channel 3 units to event CH3-E2, with about 1.2 m of horizontal slip.

3.3.4. Channel 4

The stratigraphic units in Channel 4 are numbered 400–499, from youngest to oldest, and represent nearly continuous deposition of sand, gravel and clayey sandy silt across the fault for several hundred years, as exposed in trenches T30, T31, T33, T34, T37, T39, T41, and T42. Captured within the strata of Channel 4, Wechsler et al. (2014) documented evidence for up to six paleo-earthquakes based on upward fault terminations, folding and angular unconformities. Channel 4 crossed the fault in an area where a long, linear and narrow pressure ridge is interpreted to have caused localized uplift east of the main fault, while west of the main fault, local subsidence caused the thickening of sediments (see logs for T37 and T39, Figs. 6 and 8 in Wechsler et al., 2014). There is a locally significant, down-to-the-west component of vertical motion across the entire fault zone, and local uplift along the long, linear pressure ridge within the fault zone, resulting in an apparent but lesser down-to-the-east component of vertical slip on the east side of the pressure ridge.

Channel 4 sediments range in age from at least as early as the 1st century CE up through the 4th century CE, although the lowermost

sandy gravel of channel 4 remains undated. Lower strata of Channel 4 may extend back into the latest part of the 3rd millennium BP, as its age is only constrained by one sample taken from an older channel below channel 4 that dates to the middle of the 3rd millennium BP. In fault parallel exposures, the strata are progressively older to the south on the west side of the fault based on off-lapping stratigraphic relationships revealed in fault-parallel trenches T33 and T41a. This is consistent with a model where the fault's left-lateral motion during the period of channel flow created a progression of overlapping sub-channels west of the fault, from the oldest in the south to the youngest in the north (See Figs. 7 and S1c in Wechsler et al., 2014 which describe the log of T33E, and Fig. S1k).

East of the fault, Channel 4 units are divided into two different sub-channels, located about 3 to 5 m apart. The southern channel corresponds to the older sandy-gravelly units of Channel 4 (units 490–499), which are intensely faulted, tilted and possibly eroded by younger units above them. The amount of horizontal offset for this package of sediments is difficult to determine due to their limited appearance west of the fault. We can estimate a horizontal offset of about 6.3 m based on channel reconstruction, but this should be considered a minimum value because of post-channel deformation and erosion (Fig. 5).

The northern channel corresponds to the whitish gravelly sand of units 430–439 west of the fault that are present above event CH4-E3 (Wechsler et al., 2014). This unit package is exposed in trench T39 across the fault, where it is faulted in several places, and in trenches T34 and T41, where it is tilted to the north. In trench T31, the westernmost exposure, the channel does not display any apparent tilting or folding. In order to reconstruct the flow of this sub-channel across the fault, we used both the thalweg shape based on the contact between the unit package and the sediments below it, and the thickness of the sediment package (isopach mapping), assuming that the thickest part of the channel represents the thalweg geometry before it was tilted or folded (Fig. 6). The location of the channel as inferred from the shape reconstruction yields a horizontal offset estimate of 7 ± 0.8 m, and the one inferred from the isopach reconstruction yields a larger offset estimate of 8.8 ± 0.8 m. The shape reconstruction may underestimate the amount of offset because of the tilting of the sediments west of the fault. On the other hand, the isopach reconstruction may be affected by erosion from the deposition of overlying units composed of sandy-gravely clays, which will change the apparent thickness of the mapped sediments. Due to these uncertainties we assign a horizontal offset estimate of 7.9 ± 1.7 m (the large uncertainty reflects the large difference between the upper and lower offset estimates). The vertical offset for both sub-channels is about 1.5 m.

The offset estimate for the younger units of Channel 4 is larger than the estimate for the older units, which is untenable, especially given the evidence for four surface rupturing events between the two unit packages (Wechsler et al., 2014). This inconsistency is most likely due to the underestimation of offset (6.2 m) from the lower units due to erosion of units 490–499 west of the fault.

The difference in horizontal offset between Channel 3 ($4.0^{+0.5}/_{-1.3}$ m upper Ch3, $5.2^{+0.9}/_{-0.3}$ m lower Ch3) and Channel 4 (7.9 ± 1.7 m) is attributed to the two youngest events recorded in Channel 4 sediments, both dated to the mid-3rd to mid-4th century CE. There may be a younger event between CH4-E1 and CH3-E2, for which we do not see evidence in the trenches. This difference of $2.7^{+2}/_{-2.5}$ m of lateral offset could be divided between two or three surface ruptures.

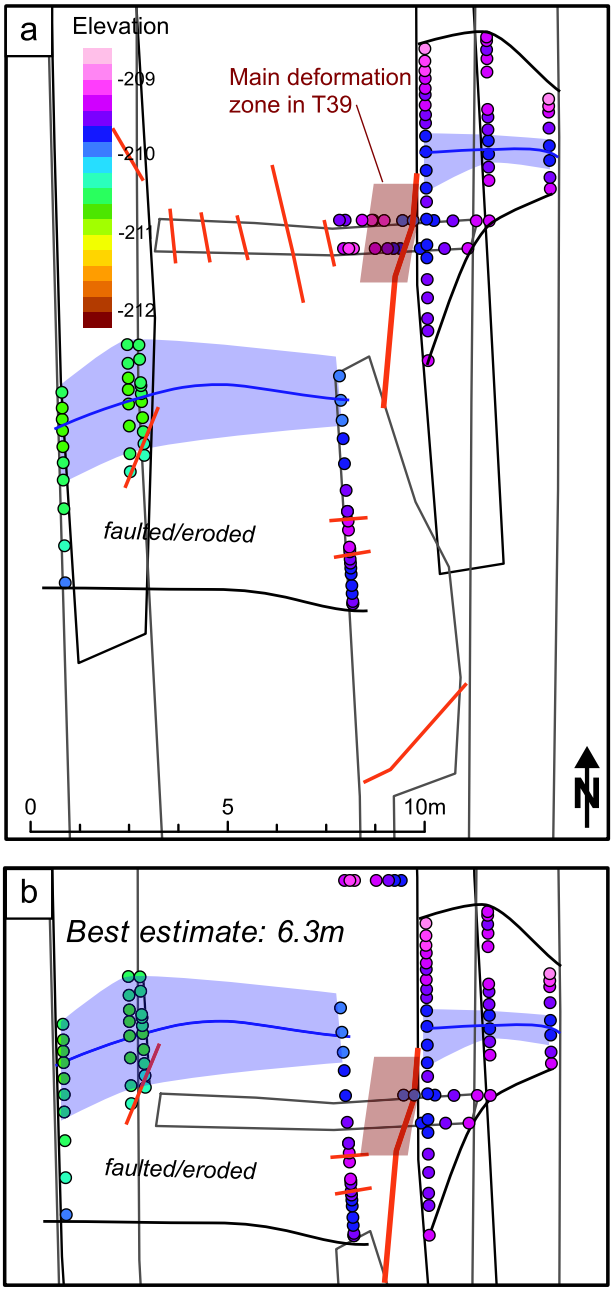

Fig. 5. Offset reconstructions for channel 4, units 490–499. Trench walls are marked by thin black lines, faults by red lines, channel margins by thick black lines, and thalweg by blue lines and blue areas. Horizontal offset reconstructions are written at the bottom left of each panel. Filled circles are actual measurement points of channel shape and their fill corresponds to the elevation. We could not generate a representing surface west of the fault due to removal by erosion/faulting of the sediments. a) Overview map of the trenches and channel. b) Reconstruction based on channel thalweg and south margin. (For interpretation of the references to color in this figure legend, the reader is referred to the web version of this article.)

3.3.5. Channel 5

Channel 5 was crossed by one trench (T30) east of the fault. It is gravel-filled, has a v-shaped form and is possibly man-made, as v-shaped excavations were common forms for early drainage canals. The channel fill was dated to the 1st–3rd century CE. We did not expose this channel west of the fault and do not discuss this channel further.

3.3.6. Channel 6

In many trenches (T30, T31, T33, T34, and T41) we encountered distinctive red-clay horizons, rich in burned organic material, which we speculate were caused by massive brush fires. East of the fault, trenches exposed a channel form filled with white gravel overlain by one or two

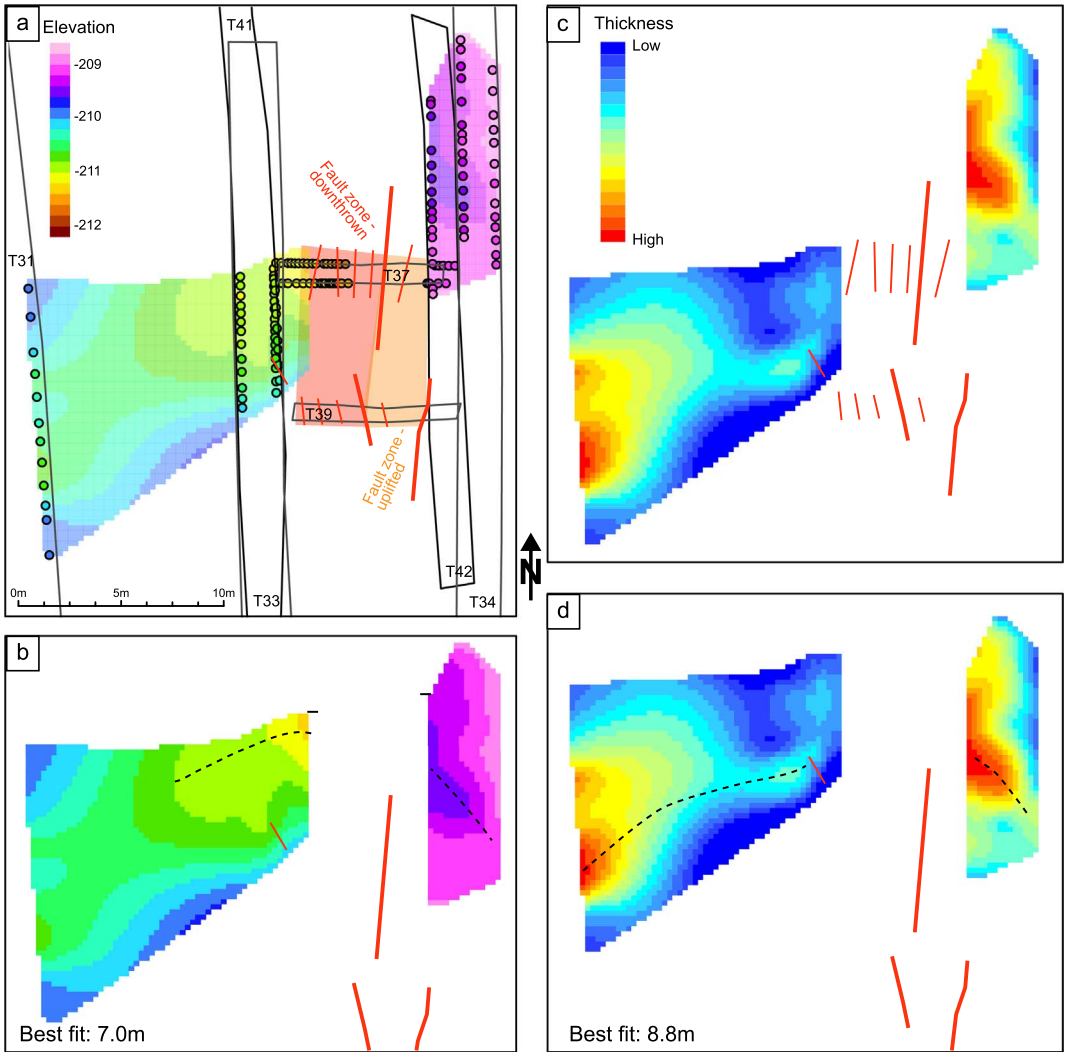

Fig. 6. Offset reconstructions for channel 4, units 430–439. Trench walls are marked by black lines, faults by red lines. Horizontal offset reconstructions are written at the bottom left of each panel. Reconstructed surfaces are color-coded by elevation; scale is the same for all figures. a) Overview map of the trenches and channel. Filled circles are actual measurement points of channel shape and their fill corresponds to the elevation. b) Reconstruction based on channel shape and north margin (the south margin west of the fault is not well defined so the reconstructed surface is truncated). c) Thickness (isopach) map of the units. d) Reconstruction based on thickness map. (For interpretation of the references to color in this figure legend, the reader is referred to the web version of this article.)

burn horizons and separated by a clean purple-brown clay unit (for example, see log of trench T34 in Fig. S1g) but we could not find a corresponding well-defined channel west of the fault. This could be explained because of the limited depth of the western trenches. We did encounter a burned horizon (red layer) west of the fault, about 2 m deeper than its likely counterpart on the east side, but the lower gravels confined to a distinct channel form were apparently too deep and were not exposed in the trenches. The burned horizon appeared to be more of a surface rather than associated with a distinct channel. Consequently, we couldn't resolve a good piercing point to follow across the fault so we do not make an estimate of lateral displacement. The burned horizon did yield several charcoal samples, and the dates yielded ages that ranged between 2840 and 2330 years BP.

3.3.7. Channel 7

Channel 7 is located farther south with respect to channels 1 to 4, and was exposed in trenches T30, T46, T47, T48, T49 and T51. Its upper part was previously excavated by Marco et al. (2005) and dated to about 5 ka BP based on bulk carbon dating. We excavated a deeper, and therefore older, part of the same channel across the fault. The channel that we mapped flows in a different direction to that described by Marco et al. (2005) and we therefore assume that its flow was interrupted, possibly by an earthquake, and changed its course from a northwest-flow direction to a southwest flow direction.

Reconstruction of the channel form yielded a well-constrained horizontal offset of 14.3 ± 1.3 m (Fig. 7). The vertical offset was only about 1 m, a lower value than for most of the other younger channels, and indeed in this locality the overall fault scarp was lower and consistent with a smaller vertical component. We attribute this to lateral variations in vertical slip along strike, although we cannot preclude the effects of erosion within the channel during successive displacements.

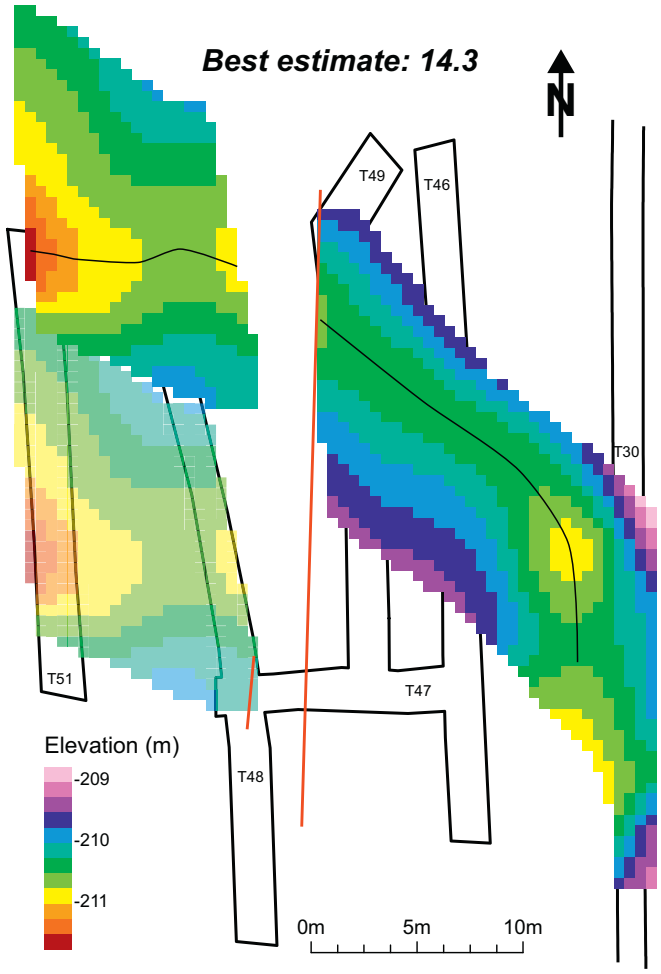

Fig. 7. Offset reconstructions for channel 7. Trench walls are marked by thin black lines, faults by red lines. Reconstructed surfaces are color-coded by elevation. The original channel shape west of the fault is semi-transparent. (For interpretation of the references to color in this figure legend, the reader is referred to the web version of this article.)

4. Results

4.1. Earthquake history from channel offsets

Table 3 and Fig. 8 summarize the event ages and the offsets attributed to each event. The earthquake ages were used for calculating the mean recurrence time between events and the corresponding coefficient of variation on timing (CV_t), using a Monte-Carlo approach: the probability density functions (pdfs) of event ages are sampled thousands of times and the mean μ, standard deviation σ and CV_t are calculated on the sampled set (Biasi, 2013; Zielke et al., 2015). The resulting mean recurrence time is 190 years and the CV_t is 1.05 (Fig. 8b), which implies elevated periods of seismic activity followed by periods of quiescence, or clustered behavior. In the following section we discuss our results in light of the historical record of earthquakes and the known paleoseismic record on neighboring faults.

The 1759 CE and 1202 earthquakes have 0.5 and 2.2 m of horizontal displacement attributed to them, respectively; the 1202 offset is the largest slip-per-event recorded at the site. The pre-1202 offset of Channel 2 of about 1.3 m is interpreted to represent slip in one moderately large earthquake. Channel 3 records one moderately large slip event of about 1.2 m, and possibly one additional small earthquake based on the cross-fault stratigraphy (Wechsler et al., 2014), although the displacement is virtually the same as that of Channel 2 suggesting that events CH2-E1 and CH3-E1 are the same event as indicated by their nearly identical ages.

Deposits in Channel 4 record evidence for six earthquakes in addition to those of Channels 1 through 3 (Wechsler et al., 2014); two of them affected the upper units with resolved additional cumulative slip $2.7^{+2}/_{-2.5}$ m. Likely both are moderate in size, each with about 1.3 m of horizontal slip, although it is possible that one of the two events may have significantly larger offset, as in 1202 CE, while the other may be a smaller, 1759-style event. We cannot rule out the possibility that there may be > 2 events that contributed to the difference in offset between channels 3 and 4, but we lack records for such events due to a disconformity in the deposition sequence.

From historical records and paleoseismology, the Yammouneh segment ruptured in 1202, between 405 and 945 CE and between 30 BCE and 469 CE (Daëron et al., 2007; Fig. 8). The penultimate Yammouneh rupture could be one of the mid-8th century earthquakes (CH2-E1 or CH3-E1, which are probably the same event). During that period, three distinct earthquakes occurred in the region and were felt from Syria in the north to Petra in the south (Fig. 1a): the first around 746 CE, the second in 749 CE and the third around 757 CE, and while the second of which most likely ruptured the Jordan Valley segment, the first or the third could have been associated with the Yammouneh fault (Ambraseys, 2005, 2009).

The JVF is interpreted to have ruptured in the earthquakes of 1033 CE, 749 and 363 based on both paleoseismic and historical records (Alfonsi et al., 2013, Ambraseys, 2009, Ferry et al., 2011, Fig. 8). Thus, the events with resolved offset at the Beteiha site could have

Table 3
Modeled earthquake dates and offset estimates for each. Historical candidate earthquakes that could have caused the offset are listed based on modeled age.[a]

Event	Modeled age	Historical	Offset estimate	Originating segment
1759 CE	–	–	0.5 m (Marco et al., 2005)	Rachaya
1202 CE	–	–	2.2 m (Marco et al., 2005)	Yammouneh
CH2-E1	675–801 CE[b]	746/749, 757 CE	1.3 m	JVF - 749 CE?
(*CH3-E1*)[c]	(*662–757 CE*)	(*659 CE*)	(*Small*)	*JGF*?
CH3-E2	505–593 CE	502, 551 CE	1.2 m	Yammouneh penultimate?
CH4-E1	294–369 CE	303, 347, 363 CE	2.7 m for 2 events	JVF – 363 CE?
CH4-E2	269–329 CE	303, 347 CE	2.7 m for 2 events	Yammouneh 3rd event?
CH4-E3	250–310 CE	303 CE	Unknown	?
CH4-E4	165–236 CE	none	Unknown	?
CH4-E5	137–206 CE	130 CE	Unknown	?
CH4-E6	392 BCE–91 CE	Mid-2nd century BCE, 92 BCE, 31 BCE, 33 CE	Unknown	?

[a] Sources for historical earthquakes include Ambraseys (2009), Amiran et al. (1994), Guidoboni (1994).
[b] Date changed from Wechsler et al. (2014).
[c] Assuming a small event that caused the avulsion on Channel 3.

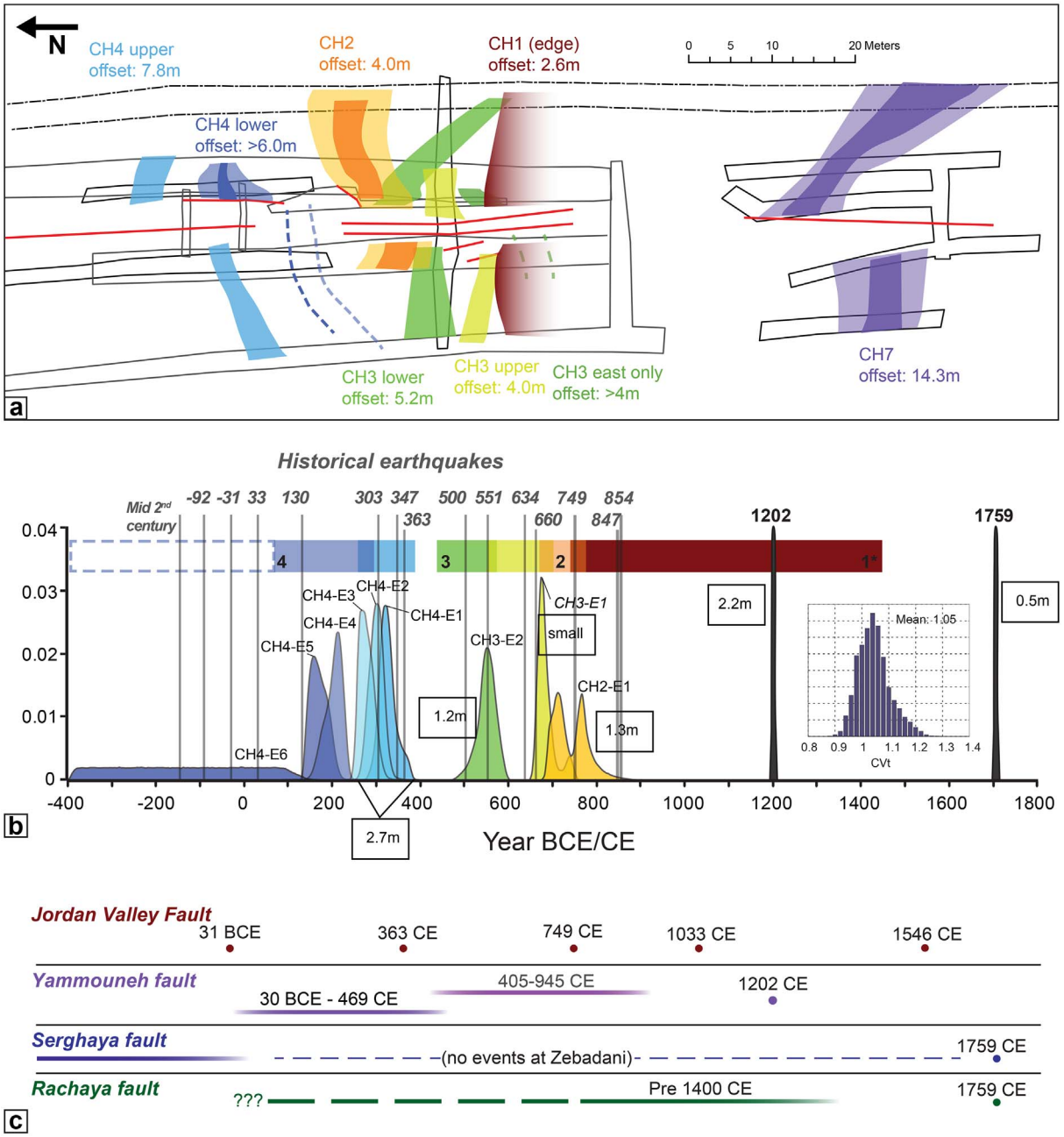

Fig. 8. a) Generalized map of the channels and their associated offsets. b) Tying the offsets to event ages. The events that were recognized by Wechsler et al. (2014) are represented by their age probability density functions (pdfs) as generated by Oxcal, and color coded by channel. For each event, an associated offset is attached. Colored boxes at the top represent the age extent of each channel's sediments. Historically known earthquakes are marked by grey lines. There is an age uncertainty as to the age of the oldest units in channel 4 (units 490–499) marked by a dashed rectangle. Inset – the result of the CVt calculation for the earthquake ages. c) Earthquakes known to have occurred on neighboring fault segments, either from historical records (dots) or from paleoseismic records (lines representing uncertainty in age). Based on figure 13 from Daeron et al. (2007). (For interpretation of the references to color in this figure legend, the reader is referred to the web version of this article.)

originated from either moderate to large events to the north or south, or from local earthquakes on the Jordan Gorge segment of the DST. This does not mean that the Jordan Gorge fault ruptured at precisely the same time, as historical records often refer to an earthquake as lasting for weeks or months and a large aftershock on the Jordan Gorge fault could have been amalgamated into the main-shock event. Thus, the observed displacements that we document here (CH2-E1) could have been coseismic with a well-known historical event or they could have been separate events that were induced or triggered by the larger regional events, although in this case the displacement may be smaller than the detection threshold of this study.

The first event documented by Wechsler et al. (2014) in channel 3 sediments (CH3-E1) is considered either quite small (less than 0.5 m offset) or the same as CH2-E1, as discussed above. The lack of datable material from the capping units prevents dating the CH3-E1 event horizon more accurately and distinguishing between it and CH2-E1.

Assuming that CH3-E1 is a separate small event that caused the channel to avulse, we use the dates from Channel 2 as the upper bound and date it to the mid-7th to mid-8th century CE (Table 2, Fig. 4). The two candidate historical earthquakes for that period are the 632/634 CE and the 659/660 CE events. The 634 earthquake occurred concurrently with the appearance of a comet, causing great consternation yet little damage in the area (Ambraseys, 2009; Guidoboni, 1994). The 660 earthquake caused extensive damage in the Jordan valley and damage in settlements throughout the region. The earthquake most likely ruptured at least part of the JVF and had documented strong aftershocks (Ambraseys, 2009).

The second event seen in channel 3 sediments (CH3-E2) dates to the 6th century CE. During that period of time several earthquakes are known to have caused damage in the region, including the 502 CE and 551 earthquakes. Both earthquakes caused damage mostly on the Lebanese and Palestinian coast, and according to damage reports, the 551 event was the stronger of the two earthquakes (Ambraseys, 2009). Paleoseismic studies point to the offshore Lebanese thrust system as the most likely source of the 551 earthquake (Elias et al., 2007), and it is possible that such a large event (estimated magnitude 7.5, Ben-Menahem, 1979) may have triggered movement on the JGF via the Roum fault, where paleoseismic evidence places the most recent event sometime after 84–239 CE (Nemer and Meghraoui, 2006). The 4th–8th century period is relatively well documented historically, so a historically "missing" event with > 1 m of slip is not likely (Zohar et al., 2016), so we interpret CH3-E2 as either associated with the 502 CE or 551 earthquakes.

The two youngest events in channel 4 sediments, CH4-E1 and E2, are associated with $2.7^{+2}/_{-2.5}$ m of offset. This amount may represent two events of comparable magnitude, similar to the channel 3 and channel 2 offsets, or it may represent one larger and one smaller event, similar to the 1202 and 1759 CE offsets. There may even be an additional event between channel 4 and channel 3, which contributes slip to the overall measured offset, although evidence for such an event is lacking due to a gap in the sediment record (Fig. 8). Candidate earthquakes that caused the offset include historical events in the 303, 347 and 363 CE. The 303 earthquake caused damage mostly along the southern Lebanese coast whereas the 347 earthquake caused local damage that is only reported from Beirut, Lebanon. The 363 event was actually 2 earthquakes that caused extensive damage in the region, from Aqaba and Petra, Jordan, south of the Dead-Sea (Klinger et al., 2015) all the way to Paneas, north of the Sea of Galilee, and most likely one of them ruptured the Jordan Valley segment. Archaeological excavations in Sussita, east of the Sea of Galilee, revealed major destruction of an Odeion and Roman basilica, where coins found beneath the collapsed structures are dated to as late as 362 CE (Wechsler and Marco, 2017). It is reasonable to assume that the 363 earthquake rupture reached as far north as the Beteiha valley and that it is part of the measured $2.7^{+2}/_{-2.5}$ m offset of the youngest two events in channel 4.

4.2. Slip per event

In order to quantify the variability of slip per earthquake, we used the measured offset estimates and error margins for the past 6 events (excluding the doubtful CH3-E1) to calculate the coefficient of variation on displacement (CV_s), using the same approach we used for the CV_t calculations. The slip in events CH4-E1 and CH4-E2 together was assumed to sum up to a total of 2.7 m, but in one sampling run we set one event with 2.2 m of slip and the other with only 0.5 m, while in the second run we set both events to have 1.3 m of slip each. Lastly, we also calculated CV_s for the last 4 events only. In all cases, the calculated mean slip-per-event was 1.2–1.3 m, with a CV_s of 0.5–0.65, which implies fairly characteristically-sized slip events. Zielke et al. (2015) attribute the low variability of slip to the nature of the dataset they examined (offset geomorphic structures along the fault) and its inability to record offsets that are smaller than some threshold (approx. 1 m). The higher values of CV_s in this study may represent a difference in resolving power, and because we were able to resolve smaller offsets and attribute them to single events our dataset includes more variability. The observation of Zielke et al. (2015) that CV_s is smaller than CV_t is valid for this study as well. This likely reflects a fundamental characteristic of the JGF, which is seemingly unable to produce large offsets per event such as recorded on neighboring faults such as the Yammouneh fault to the north.

The variability in the amount of slip associated with the different events at the Beteiha site, most of which are about 1.2–1.3 m but which range from 0.5 m to > 2 m, may reflect the different sources of earthquakes on different segments. Based on the historical record combined with the paleoseismic data, the JGF segment appears capable of rupturing in conjunction with its northern and southern neighbors as well as by itself. For example, the 1202 CE earthquake that ruptured primarily the Yammouneh segment in the Bekka Valley (Daëron et al., 2007) also produced slip as far south as the Sea of Galilee, with 2.2 m at the Beteiha site. The 1759 CE earthquake of October (M6.6) ruptured along the Jordan Gorge and the Rachaya faults, and its epicenter was probably located south of the Hula basin (Ambraseys et al., 1994; Gomez et al., 2003; Gomez et al., 2001; Nemer et al., 2008; Sbeinati et al., 2005), and produced 0.5 m of slip at both the Beteiha site (Marco et al., 2005) and the Ateret fortress (Ellenblum et al., 1998). We interpret the ~1.3 m of offset of Channel 2 and upper Channel 3 to have occurred in the mid-8th century CE. To the south, the 749 CE earthquake is interpreted to have ruptured the Jordan Valley segment based on historical reports of damage and paleoseismology (Ferry et al., 2011). Our mid-8th century event could be synchronous with the large (M7.5) 749 Jordan Valley earthquake, which extends the northern limit for this event, or it could have ruptured as a triggered event and been amalgamated into the 749 CE event, or it may represent rupture in the 746 CE or 757 CE events, both of which are interpreted to have ruptured faults north of the Beteiha Valley (Ambraseys, 2009).

4.3. Fault geometry

In order to test the feasibility of multi-segment ruptures on the JGF, a simplified model of the DST from the Jordan Valley segment to the Lebanese restraining bend (not including the Mt. Lebanon thrust) was constructed for Coulomb stress modeling. Fault orientations, dips and locking depths were taken from the literature or assumed based on surface geometry and topography (Table S1). The kinematics of the fault movement were estimated based on existing literature and fault geometry (see Table S1). We did not incorporate a creeping section along the northern JVF, to keep the model simple. In each model run, a rupture was initiated on one fault, based on displacement estimates for the last earthquake on that fault. The resulting Coulomb Stress change on the neighboring faults was calculated using Coulomb 3.3 code (Toda et al., 2011). For comparison, the typical stress drop in a surface-rupturing earthquake can range between 0.5 and 50 MPa (Allmann and Shearer, 2009), and an increase of as little as 0.1 MPa (1 Bar) in the Coulomb stress is considered in the literature as effective for triggering earthquakes (King et al., 1994). It was found that the stress increases by at least 0.1–0.2 MPa on the JGF in all cases of rupture on nearby faults, and most strongly for large events originating on the Yammouneh or Jordan Valley faults (Fig. 9). Additionally, the model demonstrated that a large earthquake on the Yammouneh fault would un-stress and therefore delay the other Lebanese faults. The coulomb stress transfer model, while being very simple, still shows how the JGF location makes it primed for offset in the event of rupture of a nearby fault, which explains the relatively large number of moderate events observed from the trench data.

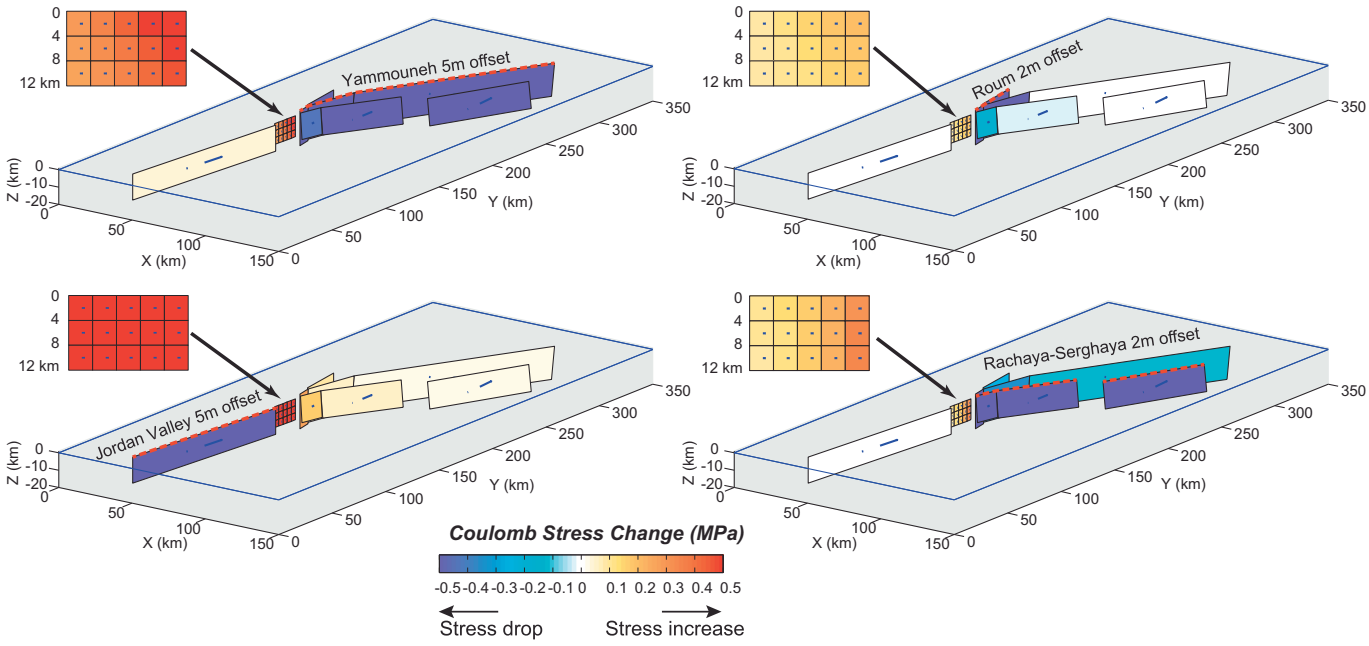

Fig. 9. Coulomb Stress modeling (using Coulomb 3.3, Toda et al., 2011) of the area using a simplified fault model of the DST from the Jordan Valley segment to the Lebanese restraining bend (not including the Mt. Lebanon thrust). In each model, an earthquake was applied on one fault (marked in dashed red line), based on rupture estimates for the last earthquake on that fault (left-lateral strike slip). The resulting Coulomb Stress change on the neighboring faults was calculated. See Table S1 for model parameters of each run. (For interpretation of the references to color in this figure legend, the reader is referred to the web version of this article.)

Ellenblum et al. (1998, 2015) excavated the archaeological site of Ateret (Vadum Iacub), which was constructed across the JGF about 12 km north of our paleoseismic site. They found an early Hellenistic (333–143 BCE) wall that was offset 6 m, and another late Hellenistic (143–63 BCE) wall that was estimated to be offset only 3.5 m. At our site, the cumulative offset for the last 1700 years is at least 7 m, and based on the overall slip rate it should be about 8–9 m for Hellenistic period features. It would be expected that the two sites would have similar amounts of displacement for similar amounts of time, yet the Ateret site appears to accommodate a lesser amount of cumulative slip, even ignoring the extremely low estimated offset of the late Hellenistic wall. This is also true for the 1202 CE rupture offset, estimated to be 1.5 m at Ateret, versus 2.2 m at the Beteiha site. This difference of ~30% less slip at the Ateret site may be explained by its location astride a branch of the JGF which is near a trifurcation point and some of the offset is taken by other branches (Fig. 9). A normal fault branches to the north-west immediately south of the archaeological site, causing a left bend in the Jordan River and offsetting Pleistocene strata. Additionally, a fault strand parallel to the Ateret branch and marked as the main continuation of the JGF northward is mapped just north of the junction, east of the site (Fig. 10). Those faults and perhaps other unknown fault(s) that are immediately adjacent to the archaeological site may accommodate some of the offset. This is supported by GPS campaign data across the JGF south of the Ateret site and the branching point, which indicate a locked fault with a slip rate of 4.1 ± 0.8 mm/yr (Hamiel et al., 2016), in agreement with the paleoseismic slip estimates from the Beteiha site (this study).

We resolved slip per event for the past six surface ruptures at the Beteiha paleoseismic site, with slip estimates ranging from 0.5 to 2.2 m, a factor of more than four (Table 3) and a corresponding CV_s value of 0.5–0.6. Although at first glance, this range of offsets argues against the characteristic earthquake model (Schwartz and Coppersmith, 1984), when local and regional structure is considered, the model may still apply in some cases. For instance, the largest displacement is associated with the 1202 earthquake, which is known to have ruptured the Bekka Valley with several meters of displacement (Daëron et al., 2007). The Beteiha site may be near the southern terminus of the 1202 rupture, although it is not known whether the rupture terminated in the Sea of Galilee or propagated as far south as the Jordan Valley. As mentioned earlier, the crusader fortress of Belvoir, located only 13 km south of the Sea of Galilee, was not damaged in the 1202 earthquake indicating that rupture did likely stop at the Galilee releasing step. In contrast, damage from the October 1759 earthquake rupture is centered on the Jordan Gorge fault (Ambraseys and Barazangi, 1989; Sieberg, 1932), and 50 cm of offset at Ateret is attributed to this event, suggesting that this event ruptured only the short, 40 km-long segment of the DST that includes the Jordan Gorge and the east side of the Hula Valley until the NE-bend in the fault, or perhaps even only the 20 km long JGF. Potentially, this earthquake may have also ruptured the Rachaya fault in Lebanon (Daëron et al., 2005), although conversely, it is possible that the Rachaya ruptured together with the Serghaya fault in the larger November 1759 event (Gomez et al., 2003). Thus, one plausible model is that small, half-meter events may represent rupture of only the 20 km-long JGF, whereas the large 1.2–2.2 offsets represent displacement in larger earthquakes that ruptured either to the north (1202 CE) or south (749, 363 CE). In transition zones between simple and complex sections of plate boundary faults, repeating earthquakes with similar displacement and rupture extent (i.e., characteristic earthquakes) may be an over-simplified model that should not really be expected to conform to reality. It should be noted that resolving 0.5 m of slip is generally beyond the accuracy limits of this study, so while there may be other 1759-style rupture events, they have not been detected. It is possible that one or more of the channel 4 events are of the smaller 1759-offset type.

4.4. Slip rate

We estimate a moderate-term slip rate for this section of the DST from the offset of Channel 7. Calibrated ages for Channel 7 are between 4200 and 3400 years BP (Table 2). Sample 463 is from the bottom of the channel and does not represent the age of the channel deposits (T49E trench log, Fig. S2). We cannot distinguish between the offset of lower and upper units, but assuming that the youngest channel units are offset the same amount as the channel's thalweg, the calculated slip-rate

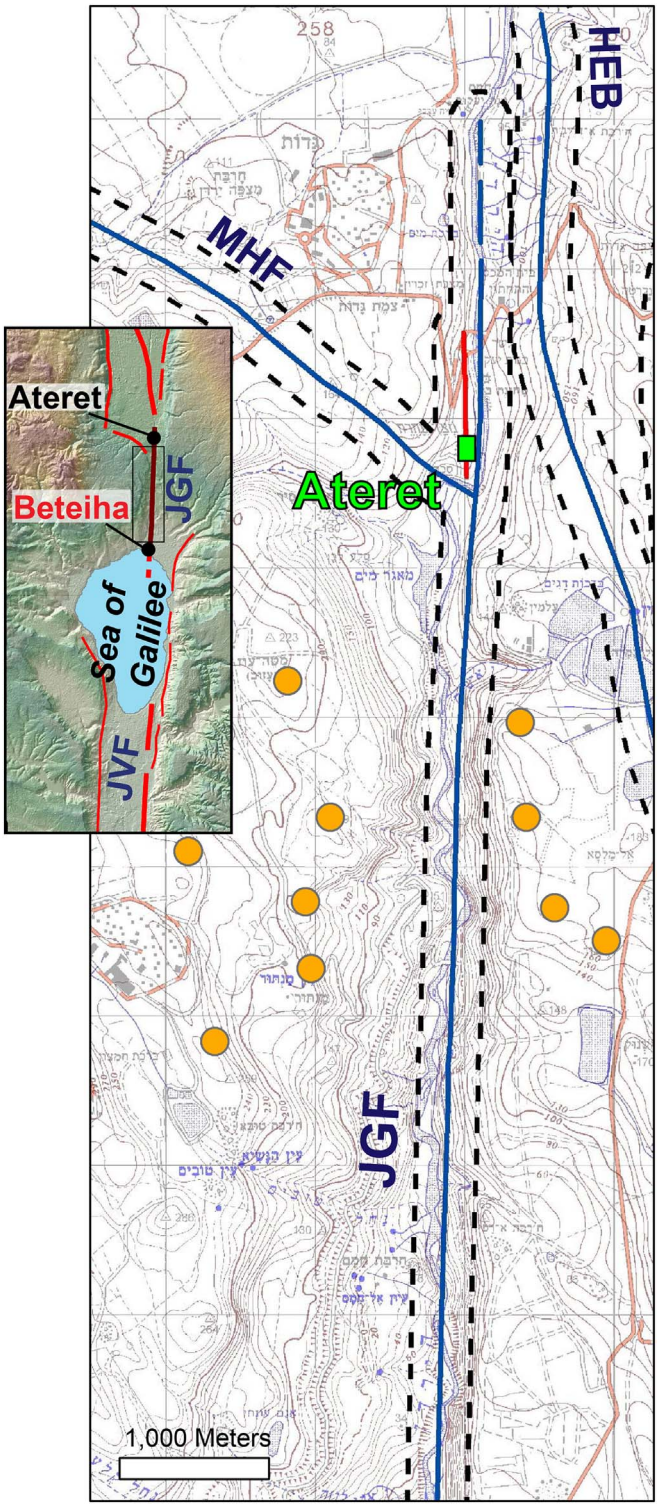

Fig. 10. An excerpt from the Israel's active fault map (Sagy et al., 2016) along the JGF. Active faults are marked in red, suspected active in blue. Orange circles mark the near-field stations of the GPS campaign measurements locations (Hamiel et al., 2016). The Ateret crusader castle (green rectangle) is situated on top of a branch of the JGF (marked red), parallel to the main fault and north of a branching point with MHF, while the GPS array of Hamiel et al. (2016) crosses the JGF south of the branching point. The Beteiha paleoseismic site is ~4 km south of the map's lower edge. Inset – location map, black rectangle marks the extent of the excerpt from the active faults map. MHF – Mishmar Hayarden fault (normal/ss). HEB – Hula Eastern border fault (normal). (For interpretation of the references to color in this figure legend, the reader is referred to the web version of this article.)

on the fault for the last four millennia is $4.1^{+0.4}/_{-1.0}$ mm/yr. This rate assumes that the offset mostly postdates the younger units, which is reasonable as there is no evidence of flow along the fault indicating that the channel had already been abandoned when it was offset. This rate is faster than the estimated 3 mm/yr of Marco et al. (2005), but they used bulk dating which was likely affected by the inheritance problem at the site (see discussion in Wechsler et al., 2014), yielding older apparent ages, and therefore slower apparent rates.

To assess short-term variations in slip rate, we used a Monte-Carlo based slip rate calculator (Styron, 2015) to estimate the overall slip-rate, and to explore the slip rate over different periods of time (Fig. 11). The overall slip-rate came out 4.0 mm/yr, in agreement with our estimate based on the offset of Channel 7 alone. Examining the 1st and 2nd millennia separately revealed a marked difference in strain release, so much so that had we inspected the site a thousand years ago we would have calculated a rate of over 8 mm/yr for the previous millennium. Thus, the slip rate determined at the Beteiha site depends on the duration over which it is averaged, because it is based on a series of discrete offsets associated with individual earthquakes. Hence, one study may underestimate the slip-rate on a fault, while another might overestimate it, depending on whether that fault had recently undergone a hiatus or a spurt of activity. For example, Marco et al. (2005) inferred a 3 mm/yr rate for the past 800 years at the site, which we confirm, whereas we also document slip rates of 4.7 mm/yr and 4.1 mm/yr for the past 1700 and 3400 years, respectively. Conversely, both the regional decadal GPS rate (Hamiel et al., 2016) and the geologic rate (Daëron et al., 2004) are consistent with our longest-term rate, as observed in most cases along strike-slip faults (Meade et al., 2013). Similar short-period discrepancies between slip rates based on only a few discrete offsets versus rates averaged over longer time periods and/or at regional scale have been observed elsewhere (Dolan et al., 2016; Onderdonk et al., 2015; Rockwell et al., 2015; Weldon et al., 2004), suggesting that the general relation between the amount of stress released by a single event and the average stress release is not necessarily straightforward.

As a thought experiment, one should wonder if a regional GPS rate established during the last 800 years would necessarily be different from a regional GPS rate established for the previous millennium, although rates established from earthquake offsets are different. A positive answer would imply significant changes over short periods of time for the deeper processes that drive long-term plate tectonics deformation rates, which seems unlikely. Eventually, this raises the question of how long should a record be in order to best estimate the long-term fault behavior, and how does that affect fault risk assessment for slow and intermediate faults, where long-term records can be difficult to obtain. Site location can also be an important factor, as seen by the tendency of the JGF to rupture in conjunction with its neighboring segments. Moreover, the interval from which a short record is sampled may bias the interpretation of average recurrence interval to be as much as a factor of two too high or too low, as seen in the Hog Lake record on the San Jacinto fault in California during the 1st millennium vs. the 2nd millennium (Rockwell et al., 2015). These observations support the notion that slip rates, as well as recurrence intervals, determined from a series of singular earthquakes should be considered with large uncertainty unless the cumulative offset has been produced by a large number of events, and supported by multiple sites.

5. Discussion

There are several major observations resulting from this study that deserve discussion. First, despite the agreement between GPS and the longer-term geological slip rates on the DST, the past 800 years appear deficient in strain release everywhere from the Gulf of Aqaba to Lebanon. Thus, in terms of moment release, most of the DST appears to have remained locked and is accumulating elastic strain. In contrast, the preceding 1200 years or so at the Beteiha site experienced a spate of

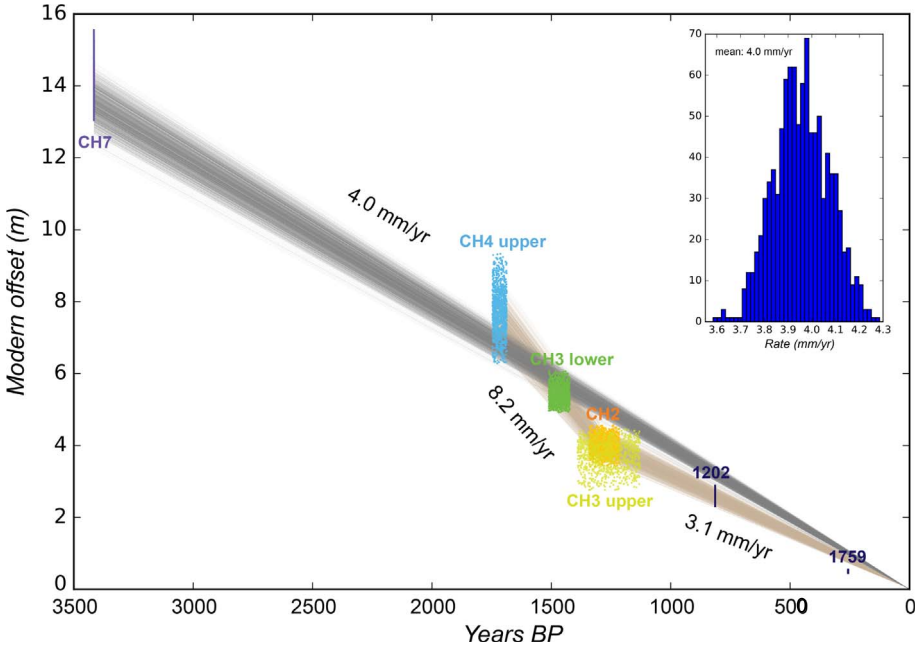

Fig. 11. Slip-rate reconstruction using Monte-Carlo methods and the slip-rate calculator by Styron (2015). The plot comprises of three separate calculations: the overall rate based on all of the measurements, and the calculated rates for the 1st and 2nd millennia separately. Inset: the histogram of slip-rate distribution for the whole data set. Each line represent a possible rate, each dot represent a possible offset value, for each channel feature. We use the youngest date from channel 7 as the lower bound for the offset age (see text for discussion).

earthquake activity, with a cluster of events that produced significant slip between about 300 and 750 CE (Fig. 12). During this 450 year "cluster", about 5 m of slip was released along the Jordan Gorge fault at the Beteiha site, yielding a short-term slip rate that exceeds a cm/yr. Thus, the slip rate on the JGF, as well as the return period, appears to have varied by a factor of two to four during the historical period, yielding a coefficient of variation (CV_t) of 1.05 on the recurrence interval, which reflects that variability. This isn't to say that the far-field strain loading has varied, but rather, that strain release in the form of fault slip has varied by a factor of two to four. This behavior is expected when the CV_t is significantly above zero, as in California where Onderdonk et al. (2015) document a factor of two variabilities in short-term slip rate for the northern San Jacinto fault, which expresses a CV_t of about 0.6.

The CV_t is a common measure of the variability in earthquake recurrence, and in California, the CV_t derived from long (> 8 events) records on sections of the San Andreas fault system yield values in the 0.4 to 0.8 range, with an average close to 0.6 (Biasi and Scharer, 2015). The value of the CV_t can vary from 0 to $CV_t > 1$, with specific ranges of CV_t values corresponding to different timing behaviors for earthquake series, from

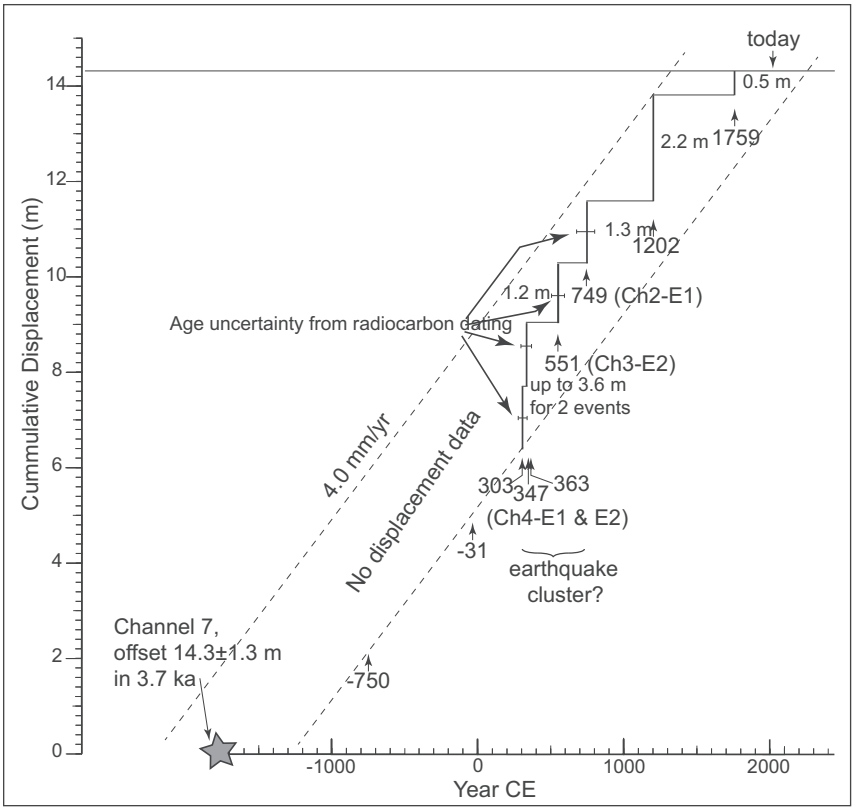

Fig. 12. Cumulative displacement vs. time based on historical earthquake dates and offsets from the reconstructed channels.

fully periodic to random to clustered (Zielke et al., 2015). The CV_t tends to be in the range of about 0.4 to 0.7 on major transform faults (Biasi et al., 2002, 2015; Biasi, 2013; Biasi and Scharer, 2015; Rockwell et al., 2001, 2009, 2015), which is still a quasi-periodic behavior but implies a non-periodic component. In contrast, a study of the activity of the Alpine fault in the central part of New-Zealand yielded a low CV_t value of 0.33 attributed to its simple geometry and high slip-rate (Berryman et al., 2012). The CV_t is important because it affects our ability to forecast future earthquakes based on the timing of occurrence of past events (Field et al., 2009, 2015, WGCEP, 2007). In some regions, the relatively high CV_t of ~0.6–0.7 may be explained by Coulomb stress loading, where a large earthquake on one fault advances or retards the timing of earthquakes on nearby faults in a complex fault array. It could also be (partly) explained by the uncertainties in dating, as paleoseismology rarely can determine the timing of a past earthquake to better than a century, so what may appear as randomly distributed earthquakes on a fault system may mask a more clustered or ordered sequence of events. This is particularly a problem on fast-moving faults, such as the San Andreas in California and the North Anatolian fault in Turkey, as the probability distributions of events ages commonly overlap because of short time intervals between successive earthquakes, dating uncertainties, and the ^{14}C calibration curve.

We interpret the high Cv_s and CV_t values as a result of the JGF interacting with its northern and southern neighboring segments, so that earthquakes nucleating to the south or to the north can either propagate into or trigger a smaller event on the JGF; the first case may have occurred in the 1202 and 1759 earthquakes and possibly also in the 551 earthquake, whereas the second case may be represented by the 363 and 749 earthquakes. This effect may result from the fact that the Beteiha site lies along a short, straight section of the DST, with relatively simple fault segments separated by releasing steps to the south and north. The northern Jordan Valley section of the DST, just south of the Sea of Galilee, exhibits some surficial creep at about half of the long-term slip rate, which suggests that the combination of the relatively small (~1 km) step in the DST at the Sea combined with the partially creeping section at the north end of the Jordan Valley may, together, be considered a potentially weak segment boundary. To the north of our site, the DST splays into at least three major faults, each of which have produced historical earthquakes (1202 on the Yammouneh fault, 1759 on the Jordan Gorge-Rachaya-Sergaya fault system, and 1837 on the Roum fault; Fig. 1b). This factor, combined with the releasing bend that produced Hula Basin north of Jordan Gorge (Fig. 1b), suggests that the Jordan Gorge section of the DST may fail on its own in moderate earthquakes, as apparently happened in October 1759.

The model that best fits the observed data for the Jordan Gorge fault is a "weak segment model", where the relatively short (20 km) JGF is bound by releasing steps (one with a component of creep) that fails on its own in moderate earthquakes or ruptures with adjacent segments. The outcome is irregular earthquake recurrence with varying amounts of displacement, resulting in significant short-term variations in slip rate. Over many earthquake cycles (8–10 or more), however, the slip rate averages out and agrees well with the geodetic and long-term geologic rates. This behavior is neither characteristic nor predictable and makes seismic hazard assessment in northern Israel more difficult. Nevertheless, as it has been over 800 years since the last large rupture, and the average recurrence interval for the past 2000 years is on the order of 250–300 years, it appears that the DST from the JGF southward to perhaps the Arava Valley is ripe for failure and should be considered as a likely source for a damaging earthquake in the geologic near-term.

6. Conclusions

Our results demonstrate that the short-term slip rate on the Jordan Gorge section of the Dead Sea fault at the Beteiha site in northern Israel has varied by a factor of two to four over the past two millennia, which we interpret to reflect the high CV_t (1.05) on the timing of earthquake recurrence rather than variations in regional loading rate. The rate for the past 3400 years is ~4.1 mm/yr, which agrees well with geodetic estimates, but there has been only 2.7 m of slip in the past millennium: this observation may portend an increase is seismic release rate in the future to "catch up" with the long term and geodetic rates. It also appears that displacement in at least 8 or 10 ruptures are needed to average out and match the long-term (geologic) and very short-term (geodetic) slip rates. This observation has important implications for slip rate studies worldwide, and argues that slip rates based on only a few earthquakes can be unreliable. The timing of past slip events argues for clustered behavior of earthquake activity, with the Jordan Gorge section as a "weak segment" that fails on its own as well as with adjacent fault segments to the north and south.

Supplementary data to this article can be found online at https://doi.org/10.1016/j.tecto.2017.10.017.

Acknowledgements

The authors would like to thank all of the people (J.B. Salisbury, E. Bowles-Martinez, P. Stepancikova, M. Buga, K. Farrington, J. Stembek, R. Gersman) who assisted with fieldwork during the trenching campaigns, and especially the landowners from Almagor who granted access to the Beteiha site. Special thanks are due to S. Marco and A. Agnon for their invaluable help. Thanks are also due to Maria Ortuño and Hector Perea for their thoughtful reviews and to the editor, JP Avouac. This project was funded by National Science Foundation Grant EAR-1019871 to T. Rockwell. N. Wechsler was partially supported by a City of Paris grant. Y. Klinger was partially supported by the Libris project (ANR-09-RISK-006).

References

Agnon, A., 2014. Pre-instrumental earthquakes along the Dead Sea Rift. In: Dead Sea Transform Fault System: Reviews. Springer, pp. 207–261.
Alchalbi, A., Daoud, M., Gomez, F., McClusky, S., Reilinger, R., Abu Romeyeh, M., Alsouod, A., Yassminh, R., Ballani, B., Darawcheh, R., Sbeinati, R., Radwan, Y., Al Masri, R., Bayerly, M., Al Ghazzi, R., Barazangi, M., 2010. Crustal deformation in northwestern Arabia from GPS measurements in Syria: slow slip rate along the northern Dead Sea Fault. Geophys. J. Int. 180, 125–135.
Alfonsi, L., Cinti, F.R., Ventura, G., 2013. The kinematics of the 1033 AD earthquake revealed by the damage at Hisham Palace (Jordan Valley, Dead Sea Transform Zone). Seismol. Res. Lett. 84, 997–1003.
Allmann, B.P., Shearer, P.M., 2009. Global variations of stress drop for moderate to large earthquakes. J. Geophys. Res. Solid Earth 114.
Ambraseys, N.N., 2005. The seismic activity in Syria and Palestine during the middle of the 8th century; an amalgamation of historical earthquakes. J. Seismol. 9, 115–125.
Ambraseys, N.N., 2009. Earthquakes in the Mediterranean and Middle East. Cambridge University Press, New York.
Ambraseys, N.N., Barazangi, M., 1989. The 1759 earthquake in the Bekaa valley: implications for earthquake hazard assessment in the eastern Mediterranean region. J. Geophys. Res. 94, 4007–4013.
Ambraseys, N.N., Melville, C.P., Adams, R.D., 1994. The Seismicity of Egypt, Arabia, and the Red Sea: A Historical Review. Cambridge University Press, Cambridge.
Amiran, D.H.K., Arieh, E., Turcotte, T., 1994. Earthquakes in Israel and adjacent areas: macroseismic observations since 100 B.C.E. Israel Explor. J. 44, 260–305.
Ben-Menahem, A., 1979. Earthquake catalogue for the Middle East (92 BC–1980 AD). Boll. Geofis. Teor. Appl. 21, 245–310.
Ben-Zion, Y., Rice, J.R., 1993. Earthquake failure sequences along a cellular fault zone in a 3-dimensional elastic solid containing asperity and nonasperity regions. J. Geophys. Res. Solid Earth 98, 14109–14131.
Berryman, K.R., Cochran, U.A., Clark, K.J., Biasi, G.P., Langridge, R.M., Villamor, P., 2012. Major earthquakes occur regularly on an isolated plate boundary fault. Science 336 (6089), 1690–1693.
Biasi, G.P., 2013. Appendix H: maximum likelihood recurrence intervals for California paleoseismic sites. In: US Geol. Surv. Open-file Rept. 2013-1165-H and Calif. Geol. Surv. Special Rept. 228-H.
Biasi, G., Scharer, K.M., 2015. Coefficient of variation estimates for the plate boundary fault system of California. In: 2015 AGU Fall Meeting.
Biasi, G.P., Weldon, R.J., Fumal, T.E., Seitz, G.G., 2002. Paleoseismic event dating and the conditional probability of large earthquakes on the southern San Andreas fault, California. Bull. Seismol. Soc. Am. 92, 2761–2781.
Biasi, G.P., Langridge, R.M., Berryman, K.R., Clark, K.J., Cochran, U.A., 2015. Maximum-likelihood recurrence parameters and conditional probability of a ground-rupturing earthquake on the southern Alpine Fault, South Island, New Zealand. Bull. Seismol. Soc. Am. 105, 94–106.
Bronk-Ramsey, C., 2009. Bayesian analysis of radiocarbon dates. Radiocarbon 51, 337–360.
Daëron, M., Benedetti, L., Tapponnier, P., Sursock, A., Finkel, R.C., 2004. Constraints on

the post-25-ka slip rate of the Yammouneh fault (Lebanon) using in situ cosmogenic Cl-36 dating of offset limestone-clast fans. Earth Planet. Sci. Lett. 227, 105–119.
Daëron, M., Klinger, Y., Tapponnier, P., Elias, A., Jacques, E., Sursock, A., 2005. Sources of the large AD 1202 and 1759 Near East earthquakes. Geology 33, 529–532.
Daëron, M., Klinger, Y., Tapponnier, P., Elias, A., Jacques, E., Sursock, A., 2007. 12,000-year-long record of 10 to 13 paleoearthquakes on the Yammouneh fault, Levant fault system, Lebanon. Bull. Seismol. Soc. Am. 97, 749–771.
Dolan, J.F., McAuliffe, L.J., Rhodes, E.J., McGill, S.F., Zinke, R., 2016. Extreme multi-millennial slip rate variations on the Garlock fault, California: strain super-cycles, potentially time-variable fault strength, and implications for system-level earthquake occurrence. Earth Planet. Sci. Lett. 446, 123–136.
Elias, A., Tapponnier, P., Singh, S.C., King, G.C.P., Briais, A., Daëron, M., Carton, H., Sursock, A., Jaques, E., Jomaa, R., Klinger, Y., 2007. Active thrusting offshore Mount Lebanon: source of the tsunamigenic AD 551 beirut-tripoli earthquake. Geology 35, 755–758.
Ellenblum, R., Marco, S., Agnon, A., Rockwell, T., Boas, A., 1998. Crusader castle torn apart by earthquake at dawn, 20 May 1202. Geology 26, 303–306.
Ellenblum, R., Marco, S., Kool, R., Davidovitch, U., Porat, R., Agnon, A., 2015. Archaeological record of earthquake ruptures in Tell Ateret, the Dead Sea Fault. Tectonics 34, 2105–2117.
Ferry, M., Meghraoui, M., Abou Karaki, N., Al-Taj, M., Amoush, H., Al-Dhaisat, S., Barjous, M., 2007. A 48-kyr-long slip rate history for the Jordan Valley segment of the Dead Sea fault. Earth Planet. Sci. Lett. 260, 394–406.
Ferry, M., Meghraoui, M., Abou Karaki, N., Al-Taj, M., Khalil, L., 2011. Episodic behavior of the Jordan Valley section of the Dead Sea fault inferred from a 14-ka-long integrated catalog of large earthquakes (vol 101, pg 926, 2011). Bull. Seismol. Soc. Am. 101, 926–927.
Field, E.H., Dawson, T.E., Felzer, K.R., Frankel, A.D., Gupta, V., Jordan, T.H., Parsons, T., Petersen, M.D., Stein, R.S., Weldon, R., 2009. Uniform California earthquake rupture forecast, version 2 (UCERF 2). Bull. Seismol. Soc. Am. 99, 2053–2107.
Field, E.H., Biasi, G.P., Bird, P., Dawson, T.E., Felzer, K.R., Jackson, D.D., Johnson, K.M., Jordan, T.H., Madden, C., Michael, A.J., Milner, K.R., 2015. Long-term time-dependent probabilities for the third Uniform California Earthquake Rupture Forecast (UCERF3). Bull. Seismol. Soc. Am. 105 (2A), 511–543.
Freund, R., Zak, I., Garfunkel, Z., 1968. Age and rate of the sinistral movement along the Dead Sea Rift. Nature 220, 253–255.
Fumal, T.E., Weldon, R.J., Biasi, G.P., Dawson, T.E., Seitz, G.G., Frost, W.T., Schwartz, D.P., 2002. Evidence for large earthquakes on the San Andreas fault at the Wrightwood, California, paleoseismic site: AD 500 to present. Bull. Seismol. Soc. Am. 92, 2726–2760.
Garfunkel, Z., 1981. Internal structure of the Dead Sea leaky transform (rift) in relation to plate kinematics. Tectonophysics 80, 81–108.
Garfunkel, Z., Zak, I., Freund, R., 1981. Active faulting in the Dead Sea rift. Tectonophysics 80, 1–26.
Gomez, F., Meghraoui, M., Darkal, A.N., Sbeinati, R., Darawcheh, R., Tabet, C., Khawlie, M., Charabe, M., Khair, K., Barazangi, M., 2001. Coseismic displacements along the Serghaya fault: an active branch of the Dead Sea fault system in Syria and Lebanon. J. Geol. Soc. 158, 405–408.
Gomez, F., Meghraoui, M., Darkal, A.N., Hijazi, F., Mouty, M., Suleiman, Y., Sbeinati, R., Darawcheh, R., Al-Ghazzi, R., Barazangi, M., 2003. Holocene faulting and earthquake recurrence along the Serghaya branch of the Dead Sea fault system in Syria and Lebanon (vol 153, pg 658, 2003). Geophys. J. Int. 155, 749–750.
Gomez, F., Nemer, T., Tabet, C., Khawlie, M., Meghraoui, M., Barazangi, M., 2007. Strain partitioning of active transpression within the Lebanese restraining bend of the Dead Sea fault (Lebanon and SW Syria). Geol. Soc. Lond., Spec. Publ. 290, 285–303.
Guidoboni, E., 1994. Catalogue of Ancient Earthquakes in the Mediterranean Area up to the 10th Century. Istituto Nazionale di Geofisica, Rome.
Hamiel, Y., Piatibratova, O., Mizrahi, Y., 2016. Creep along the northern Jordan Valley section of the Dead Sea Fault. Geophys. Res. Lett. 43, 2494–2501.
Hecker, S., Abrahamson, N., Wooddell, K., 2013. Variability of displacement at a point: implications for earthquake-size distribution and rupture hazard on faults. Bull. Seismol. Soc. Am. 103, 651–674.
Hofstetter, A., 2003. Seismic observations of the 22/11/1995 Gulf of Aqaba earthquake sequence. Tectonophysics 369, 21–36.
Kagan, E., Stein, M., Agnon, A., Neumann, F., 2011. Intrabasin paleoearthquake and quiescence correlation of the late Holocene Dead Sea (vol 116, B04311, 2011). J. Geophys. Res. Solid Earth 116.
King, G., Stein, R., Lin, J., 1994. Static stress changes and the triggering of earthquakes. Bull. Seismol. Soc. Am. 84, 935–953.
Klinger, Y., Etchebes, M., Tapponnier, P., Narteau, C., 2011. Characteristic slip for five great earthquakes along the Fuyun fault in China. Nat. Geosci. 4, 389–392.
Klinger, Y., Le Beon, M., Al-Qaryouti, M., 2015. 5000 yr of paleoseismicity along the southern Dead Sea fault. Geophys. J. Int. 202, 313–327.
Le Beon, M., Klinger, Y., Amrat, A.Q., Agnon, A., Dorbath, L., Baer, G., Ruegg, J.C., Charade, O., Mayyas, O., 2008. Slip rate and locking depth from GPS profiles across the southern Dead Sea Transform. J. Geophys. Res. Solid Earth 113.
Le Beon, M., Klinger, Y., Al-Qaryouti, M., Meriaux, A.S., Finkel, R.C., Elias, A., Mayyas, O., Ryerson, F.J., Tapponnier, P., 2010. Early Holocene and Late Pleistocene slip rates of the southern Dead Sea Fault determined from Be-10 cosmogenic dating of offset alluvial deposits. J. Geophys. Res. Solid Earth 115.
Le Beon, M., Klinger, Y., Meriaux, A.S., Al-Qaryouti, M., Finkel, R.C., Mayyas, O., Tapponnier, P., 2012. Quaternary morphotectonic mapping of the Wadi Araba and implications for the tectonic activity of the southern Dead Sea fault. Tectonics 31.
Marco, S., Rockwell, T.K., Heimann, A., Frieslander, U., Agnon, A., 2005. Late Holocene activity of the Dead Sea Transforrn revealed in 3D palaeoseismic trenches on the Jordan Gorge segment. Earth Planet. Sci. Lett. 234, 189–205.
McClusky, S., Reilinger, R., Mahmoud, S., Ben Sari, D., Tealeb, A., 2003. GPS constraints on Africa (Nubia) and Arabia plate motions. Geophys. J. Int. 155, 126–138.
Meade, B.J., Klinger, Y., Hetland, E.A., 2013. Inference of multiple earthquake-cycle relaxation timescales from irregular geodetic sampling of interseismic deformation. Bull. Seismol. Soc. Am. 103, 2824–2835.
Nemer, T., Meghraoui, M., 2006. Evidence of coseismic ruptures along the Roum fault (Lebanon): a possible source for the AD 1837 earthquake. J. Struct. Geol. 28, 1483–1495.
Nemer, T., Meghraoui, M., Khair, K., 2008. The Rachaya-Serghaya fault system (Lebanon): evidence of coseismic ruptures, and the AD 1759 earthquake sequence. J. Geophys. Res. Solid Earth 113.
Onderdonk, N.W., McGill, S.F., Rockwell, T.K., 2015. Short-term variations in slip rate and size of prehistoric earthquakes during the past 2000 years on the northern San Jacinto fault zone, a major plate-boundary structure in southern California. Lithosphere 7, 211–234.
Quennell, A.M., 1956. Tectonics of the Dead Sea rift. In: Congreso Geologico Internacional, 20th Sesion, Asociacion de Servicios Geologicos Africanos, pp. 385–405 (Mexico City).
Reid, H.F., 1910. The Mechanics of the Earthquake. Carnegie Institute, Washington D.C.
Reilinger, R., McClusky, S., Vernant, P., Lawrence, S., Ergintav, S., Cakmak, R., Ozener, H., Kadirov, F., Guliev, I., Stepanyan, R., 2006. GPS constraints on continental deformation in the Africa-Arabia-Eurasia continental collision zone and implications for the dynamics of plate interactions. J. Geophys. Res. Solid Earth 111.
Reimer, P.J., Bard, E., Bayliss, A., Beck, J.W., Blackwell, P.G., Ramsey, C.B., Buck, C.E., Cheng, H., Edwards, R.L., Friedrich, M., Grootes, P.M., Guilderson, T.P., Haflidason, H., Hajdas, I., Hatte, C., Heaton, T.J., Hoffmann, D.L., Hogg, A.G., Hughen, K.A., Kaiser, K.F., Kromer, B., Manning, S.W., Niu, M., Reimer, R.W., Richards, D.A., Scott, E.M., Southon, J.R., Staff, R.A., Turney, C.S.M., van der Plicht, J., 2013. Intcal13 and Marine13 radiocarbon age calibration curves 0–50,000 years cal BP. Radiocarbon 55, 1869–1887.
Rockwell, T., Barka, A., Dawson, T., Akyuz, S., Thorup, K., 2001. Paleoseismology of the Gazikoy-Saros segment of the North Anatolia fault, northwestern Turkey: comparison of the historical and paleoseismic records, implications of regional seismic hazard, and models of earthquake recurrence. J. Seismol. 5, 433–448.
Rockwell, T., Ragona, D., Seitz, G., Langridge, R., Aksoy, M.E., Ucarkus, G., Ferry, M., Meltzner, A.J., Klinger, Y., Meghraoui, M., 2009. Palaeoseismology of the North Anatolian fault near the Marmara Sea: implications for fault segmentation and seismic hazard. Geol. Soc. Lond., Spec. Publ. 316, 31–54.
Rockwell, T.K., Dawson, T.E., Ben-Horin, J.Y., Seitz, G., 2015. A 21-event, 4,000-year history of surface ruptures in the Anza Seismic Gap, San Jacinto fault, and implications for long-term earthquake production on a major plate boundary fault. Pure Appl. Geophys. 172, 1143–1165.
Sagy, A., Sneh, A., Rosensaft, M., Bartov, Y., 2016. Map of active faults and potentially active faults for the Israel Standard 413 “design provisions for earthquakes resistance of structures”. In: Update 2016 Israel Geological Survey, Jerusalem.
Salisbury, J.B., Rockwell, T.K., Middleton, T.J., Hudnut, K.W., 2012. LiDAR and field observations of slip distribution for the most recent surface ruptures along the Central San Jacinto Fault. Bull. Seismol. Soc. Am. 102, 598–619.
Sbeinati, M.R., Darawcheh, R., Monty, M., 2005. The historical earthquakes of Syria: an analysis of large and moderate earthquakes from 1365 BC to 1900 AD. Ann. Geophys. 48, 347–435.
Scharer, K.M., Weldon, R.J., Fumal, T.E., Biasi, G.P., 2007. Paleoearthquakes on the southern San Andreas Fault, Wrightwood, California, 3000 to 1500 BC: a new method for evaluating paleoseismic evidence and earthquake horizons. Bull. Seismol. Soc. Am. 97, 1054–1093.
Schwartz, D.P., Coppersmith, K.J., 1984. Fault behavior and characteristic earthquakes: examples from the Wasach and San Andreas fault zones. J. Geopys. Res. 89, 5681–5698.
Shapira, A., Avni, R., Nur, A., 1993. A new estimate for the epicenter of the Jericho earthquake of 11 July 1927. Isr. J. Earth Sci. 42, 93–96.
Sieberg, A., 1932. Erdbebengeographie. In: Handbuch der Geophysik, Band IV. Borntraeger, Berlin, pp. 527–1005.
Sieh, K.E., 1984. Lateral offsets and revised dates of large prehistoric earthquakes at Pallett Creek, southern-California. J. Geophys. Res. 89 (7641-&).
Styron, R., 2015. Slip rate calculator. https://github.com/cossatot/slip_rate_calculator.
Toda, S., Stein, R.S., Sevilgen, V., Lin, J., 2011. Coulomb 3.3 Graphic-rich Deformation and Stress-change Software for Earthquake, Tectonic, and Volcano Research and Teaching-user Guide. US Geological Survey.
Wechsler, N., Marco, S., 2017. Historical earthquakes in northern Israel and their impact on Susita-Hippos. Michmanim 27, 35–45.
Wechsler, N., Rockwell, T.K., Klinger, Y., Stepancikova, P., Kanari, M., Marco, S., Agnon, A., 2014. A Paleoseismic record of earthquakes for the Dead Sea Transform fault between the first and seventh centuries CE: nonperiodic behavior of a plate boundary fault. Bull. Seismol. Soc. Am. 104, 1329–1347.
Weldon, R., Scharer, K., Fumal, T., Biasi, G., 2004. Wrightwood and the earthquake cycle: what a long recurrence record tells us about how faults work. GSA Today 14, 4–10.
WGCEP, 2007. The Uniform California Earthquake Rupture Forecast, Version 2 (UCERF 2).
Zielke, O., Klinger, Y., Arrowsmith, J.R., 2015. Fault slip and earthquake recurrence along strike-slip faults - contributions of high-resolution geomorphic data. Tectonophysics 638, 43–62.
Zilberman, E., Amit, R., Heimann, A., Porat, N., 2000. Changes in Holocene paleoseismic activity in the Hula pull-apart basin, Dead Sea Rift, northern Israel. Tectonophysics 321, 237–252.
Zohar, M., Salamon, A., Rubin, R., 2016. Reappraised list of historical earthquakes that affected Israel and its close surroundings. J. Seismol. 1–15.